

Response to all referees

We would like to thank the two reviewers for the comments and suggestions, which help to improve the quality of our work. We have made revisions and have replied to all comments and suggestions. Please find a detailed point-by-point response to each comment. Our responses are shown in “Blue” color and the changes in the manuscript are shown in “Red” color.

Referee #1

Comment:

This manuscript describes a new approach to obtain SSR from satellites, and the proposed idea on how to combine MODIS and MTSAT data and offset their respective observation shortcomings indeed is very novel. Throughout the manuscript, the structure, elements, procedures, discussions and analyses all are well organized, and thereby it is fluent to read. In a word, I find the study is interesting and well sound and it is worth publishing in Atmospheric Chemistry and Physics. Even though I think the study is worth publishing in ACP, it may be still require some modifications.

Response:

We thank Referee #1 for the encouraging comments. All comments and suggestions have been considered carefully and well addressed.

Comment:

1. Generally speaking, if we want to retrieve the atmospheric states (e.g. cloud-related parameters) from satellite TOA (Top of the Atmosphere) observations, the surface states must be known or assumed in advance. However, in your method the cloud-related parameters are directly linked with TOA MTSAT observations by an ANN method. Are the fluctuations of surface states, such as different surface reflectance, required to be further accounted for in your retrieving scheme? Do you compare your cloud mask results with MTSAT TOA VIS images through visual identification, and are they in agreement each other?

Response:

I agree that the surface states must be known or assumed in advance when retrieving the atmospheric states from satellite TOA (Top of the Atmosphere) observations. This is especially significant when the air condition is clear sky, in which case the TOA radiances are affected greatly by the surface states. Under cloudy condition, the effects of clouds on TOA radiances are much greater than those of the surface states on TOA radiances. Thus, most retrieval algorithms for atmospheric states cannot work well, while the retrieval algorithms for cloud parameter are almost not affected by the surface states. Furthermore, MODIS cloud retrieval algorithm has accounted for the surface effects when retrieving cloud parameters. Therefore, we directly build relationships between MODIS cloud parameters and TOA MTSAT observations with an ANN method without considering surface states.

Yes, we randomly selected a few cloud mask pictures and compared with the corresponding MTSAT TOA VIS images through visual identification and found that they are generally in agreement with each other.

Comment:

2. You first use to MTSAT TOA 5 channel data to derive cloud parameters, and then use resulting cloud parameters to compute SSR. Why didn't you choose a more straight-forward way to obtain SSR, namely directly retrieving SSR from MTSAT TOA 5 channel data? You also can use MODIS cloud products and the algorithm of Qin et al. (2015) to obtain SSR, and then establish the direct relationship between SSR and MTSAT observations by an ANN method.

Response:

Generally, there are two types of methods to directly retrieve SSR from the MTSAT TOA channel data. One is the look-up table methods that use satellite signals to match a pre-established radiative-transfer database. These methods are widely adopted by many researchers (such as Pinker et al., 2003; Liang et al., 2006; Mueller et al., 2009; Lu et al., 2010; Huang et al., 2011; Ma and Pinker, 2012), but their computational efficiency are not high, and most of them only use visible channel data. The other is the statistical methods that directly link TOA radiance with the observed SSR at regional scale. For example, Using ANN technology, Lu et al. (2011) built the non-linear relationship between daily SSR measurements and MTSAT-1R all-channel radiances over China, and the evaluation results indicate that the relationship can efficiently estimate daily SSR from MTSAT-1R data. However, the non-linear relationship is not universal and needs local calibrations. To alleviate the weaknesses of the above methods, Qin et al. (2015) developed an efficient physically based parameterization algorithm to retrieve SSR. This algorithm can retrieve SSR quickly and be used globally. Qin et al. (2015) have applied the algorithm on polar-orbit satellite (MODIS Terra/Aqua), and this study attempts to apply the algorithm on geostationary satellite to map high spatio-temporal resolution SSR over China. To achieve this goal, we first use MTSAT TOA 5 channel data to derive cloud parameters, and then use the derived cloud parameters to compute SSR.

Your suggestion of using MODIS cloud products and the algorithm of Qin et al. (2015) to obtain SSR and then establishing the direct relationship between SSR and MTSAT observations by an ANN method may be equivalent to what we have done in this study. It is worth doing in the future.

Comment:

3. In the mid-latitude regions such as most parts of mainland China, the overpass times of Terra-MODIS and Aqua-MODIS respectively roughly are 11:00 and 13:30. Around these times, the solar zenith angles are relatively small. Therefore, the samples that you used to train ANN maybe lose representativeness for cases that solar zenith angles are large (e.g., the hours around sunrise and sunset). This may also influence your retrieval accuracy. Is this right? My questions may seem a little too

harsh, but you should try your best to response them.

Response:

Good comment! We randomly selected a large number of data points to train the ANNs for cloud parameters estimation. These data points cover most of China and span all four seasons. We have checked the training data and found that the values of solar zenith angle (SZA) vary from about 7.1° to 78.3° . This range of SZA is sufficiently wide except for extreme cases such as the hours around sunrise and sunset, but the value of SSR is very small in the extreme cases. Also, it should be noted that the angle information is not the determinative factor in retrieving cloud parameters. As a matter of fact, the question you mentioned has been discussed among the authors when designing the ANN. The above discussion has been added into the **text (L186-196)**.

Specific comments:

Comment:

1. P. 35202, L. 16: or 3.52.P. 35203, L. 26: “with inputs” may be more appropriate?

Response:

Accepted!

Comment:

2. P.35204, L. 1: Is it better to change “get their values at...” into “them with”?

Response:

Accepted!

Comment:

3. P.35204, L. 3: “their limited...” may be more appropriate?

Response:

Accepted!

Comment:

4. P.35205, L. 11: MTSAT1R is 135 degree and MTSAT2 is 140 degree, which one did you use?

Response:

MTSAT-1R is positioned at 140° E and MTSAT-2 is positioned at 145° E. In this study, both MTSAT-1R and MTSAT-2 data are used to map high spatio-temporal resolution SSR dataset (hourly, 5 km) over China from 2007 to 2014. The observed SSR data in 2009 are used to validate the retrieved SSR, which were estimated from MTSAT-1R data.

Comment:

5. P.35205, L. 25: Misleading phrase “The spatial resolutions of these MODIS products are 5 km”, different MODIS products have different spatial resolutions.

Response:

The authors are sorry for this error. The spatial resolutions of the aerosol products

(MOD04, MYD04), atmospheric profiles products (MOD07, MYD07) and albedo products (MCD43C3) are 5 km; whereas, the spatial resolution of cloud products is 1 km. Thus we resample the cloud products to a spatial resolution of 5 km in the original manuscript. This information has been added into the text (L121-124).

Comment:

6. P.35208, Sect. 3.2: Here the descriptions are a bit disordered. Maybe, the following revision is better. The conclusion “Comparison between ... To improve... train the ANN” in the end of this paragraph, is adjusted into the end of next paragraph. You respectively describe the training data and validation data, and then conclude their similar behaviors, finally all data are used to train the ANN. between the L. 15 and L. 25, and the “observed ones” is “the MODIS derived”, isn’t it? In a word, these two paragraphs need to be rephrased.

Response:

Yes, you logic is right. Actually, the logic you suggested has been briefly described in the original manuscript as “The MODIS cloud products are randomly selected, and split into two parts: one for training and other for independent validation. Comparison between the two parts indicates that the trained ANNs behave similar to each other. To improve the generalization of the ANN model, we use all the data to train the ANN”. Figure 3 and Figure 4 in the original manuscript use all the data to train the ANN. To avoid misunderstanding, we have added the text “After all the data are used to train the ANN,” into the text (L206).

Yes, the “observed ones” is the “MODIS derived ones”.

Comment:

7. P.35209, L. 23: 2.9 g cm^{-2} seems to be small. From my experience, under cloudy skies the absorption of water vapor usually is saturated. Maybe 3.5 g cm^{-2} is more appropriate.

Response:

Maybe you are right, but the PW effect is negligible under cloudy conditions because the cloud effect on the SSR is dominant. Therefore, we may expect that the using of 2.9 g cm^{-2} or 3.5 g cm^{-2} will produce negligible difference.

Comment:

8. P.35210, L. 22-24: Misleading phrase “The lack of three-dimension...”, please rephrase it.

Response:

We have changed this sentence to “The lack of three-dimensional radiative effects in the SSR retrieval algorithm and the appearance of broken clouds are the potential reasons for the hourly SSR bias” in the text (L288-290).

Comment:

9. P.35213, L. 4-5: I do agree with the reasons you presented here. “This would be

due to the coarse spectral resolution of geostationary satellites...”. I feel that maybe two factors contribute this phenomenon. One is satellite observing TOA reflectance has saturated for too thick clouds. Subsequently TOA reflectances can not reflect the change of cloud optical depth, and result in overestimated atmospheric transmittance. Another one is the “representative cloud” and “climatology average aerosol loading” are used in the calculation of SSR. This means extremely cases can not be accounted for, and a systematic underestimation in certain high value range and a systematic overestimation in certain low value range are certainly resulted in. Frankly, it is weird that GLASS SSR has such large systematic errors on a daily timescale. In summary, my overall recommendation is that this work could go further for publication provided the authors will provide a thorough rebuttal to the aforementioned issues.

Response:

I agree with you absolutely.

Referee #2

Comment:

As well known, Incident shortwave radiation (ISR) at the surface is an essential parameter in the land surface radiation budget and in many land surface process models. This manuscript entitled “Retrieving high-resolution surface solar radiation with cloud parameters derived by combining MODIS and MTSAT data” presented an effective method to retrieve ISR with cloud parameters, including effective particle radius, liquid water path, and ice water path, by combining MODIS and MTSAT data. The retrieved ISR data were also compared with ground measurements and current satellite-derived ISR products. The paper is well written and organized. Overall, I feel the paper presents interesting scientific results as the retrieval algorithm is novel and the comparisons are extensive and valuable for knowing their overall accuracies using direct measurements. However, the manuscript is lacking in detail in a few areas (see comments below for details). Therefore, I would not recommend the paper for potential publication in ACP unless substantial improvements are made to address the following concerns.

Response:

We thank Referee #2 for the encouraging comments. All comments and suggestions have been considered carefully and well addressed.

Comment:

1. As mentioned in the manuscript, the major contributions of the authors are to present an effective method to retrieve high temporal resolution cloud parameters by establishing correlations between MODIS cloud products and MTSAT TOA radiance based on ANN, since the parameterization scheme has been reported in the previous studies presented by the authors. As it is well known, one obvious advantage to use satellite data for the mapping of surface or atmospheric parameters is the fact that it is available at least regionally, potentially even on a global level. Although the authors compared the retrieved high temporal resolution cloud parameters with the MODIS

“TRUE values”, the mapping of high temporal resolution cloud parameters were not displayed in the context. I would suggest the authors to present some retrieved results of high temporal resolution cloud parameters.

Response:

Cloud covers and cloud parameters change drastically, which significantly affect SSR. In terms of SSR retrieval, it makes little sense to simply average the cloud parameters on the seasonal or annual scale. Thus, an instantaneous image of high resolution cloud parameters at 4:00UTC on July 7th, 2009 was randomly selected and displayed in Figure 1, which shows the spatial distribution of cloud parameters clearly. The figure will not be added in the manuscript, because displaying an instantaneous image of cloud parameters in the manuscript have no apparent scientific significance. As indicated in the manuscript, the accuracy of our retrieved SSR is comparable or even higher than other two radiation products (GLASS and ISCCP-FD). Therefore, we may expect that the cloud parameters derived in this study is relatively reliable.

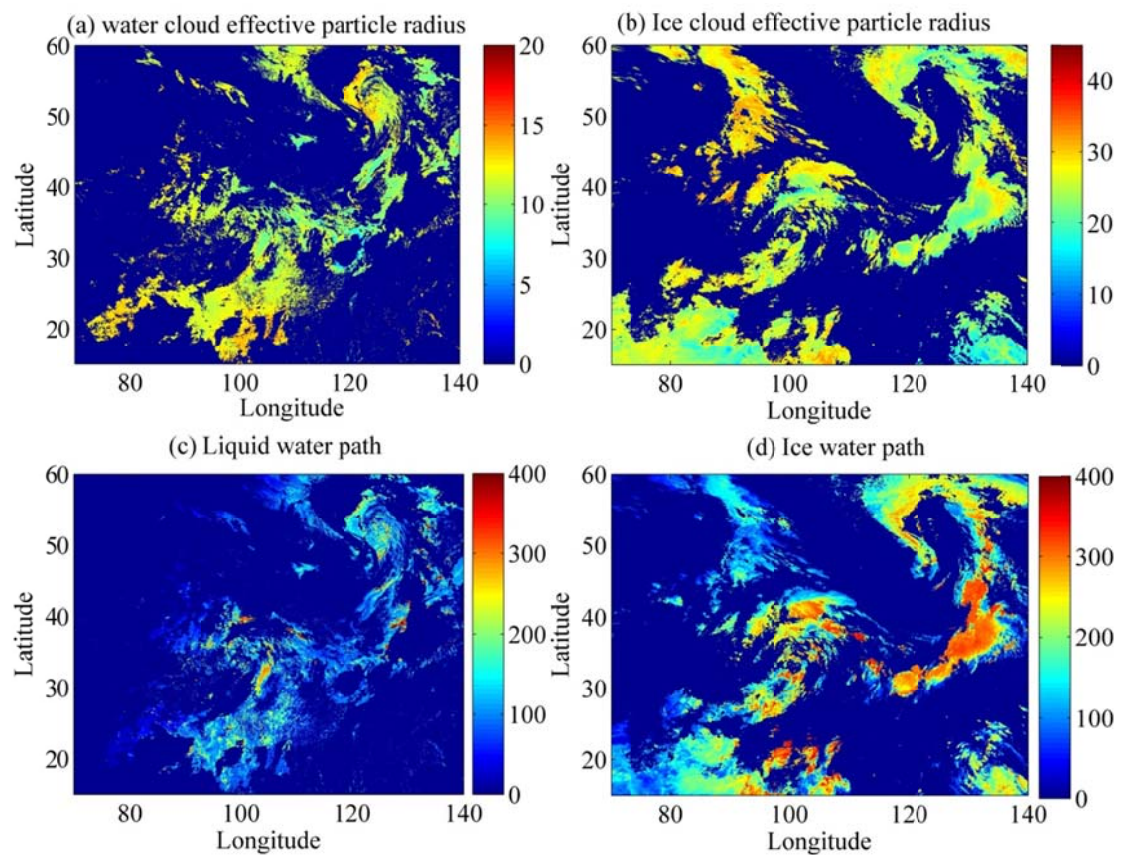


Figure 1 An example of the spatial distribution of cloud parameters at 4:00UTC on July 7th, 2009.

Comment:

2. The authors simply concluded that the overestimation in the proposed scheme might be attributed to the underestimation of the cloud water path. I think extra sensitive analyses are needed in Section 3.2. How the cloud parameters influence the retrieval accuracy?

Response:

Good comment! The sensitivity test of the SSR retrieval algorithm to cloud parameters (effective particle radius and liquid/ice water path) is presented in Figure 2. The condition used for the sensitivity test is specified as a mid-latitude atmosphere with: solar zenith angle of 60 degree, surface elevation of 0.0 km, precipitable water of 0.14 cm, total zone amount of 0.25 cm, surface albedo of 0.2 and Ångström turbidity coefficient of 0.1. We estimated the sensitivity of SSR retrieval to estimation errors in both liquid/ice water path and effective particle radius. As shown in Figure 3 and Figure 4 (in the original manuscript), the estimated mean effective particle radius within one standard deviation (1σ) correspond to the ranges of about 8-12 μm and 22-30 μm for water cloud and ice cloud, which would lead to SSR changing about 25 W m^{-2} and 15 W m^{-2} as seen from Figure 2, respectively. The estimated mean cloud liquid/ice water path within 1σ correspond to the ranges of about 45-185 g m^{-2} , 80-240 g m^{-2} , which would lead to SSR changing about 154 W m^{-2} and 172 W m^{-2} , respectively. Obviously, errors in SSR caused by the cloud liquid/ice water path estimation errors are much greater than the ones caused by cloud effective particle radius estimation errors. Therefore, we believe that the underestimation of cloud liquid/ice water path is the major cause for the overestimation of SSR.

The above information has been added in the text (L220-235).

The MBE and RMSE for cloud parameters estimation has been added on Figure 3 and Figure 4 in the revised manuscript.

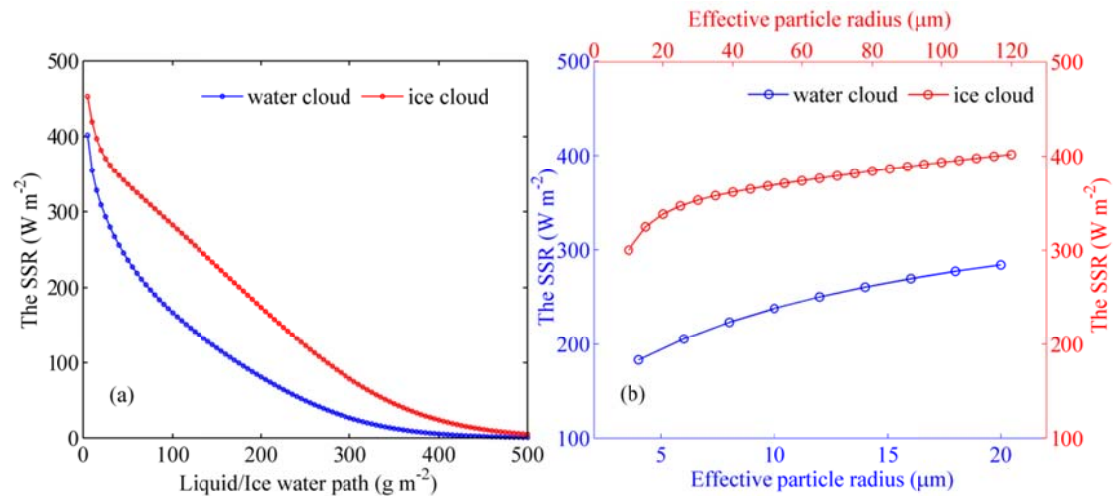


Figure 2 (a) Sensitivity of SSR to cloud liquid/ice water path, given the effective particle radius for water cloud and ice cloud to be 12 μm and 30 μm , respectively; (b) Sensitivity of SSR to cloud effective particle radius for water cloud and ice cloud, given liquid/ice water path to be 80 g m^{-2} .

Comment:

3. The spatial resolution of ISCCP-FD product is about 280 km, while the spatial resolutions the GLASS and the retrieval results based on the proposed method are 5 km. Will different spatial resolutions affect the evaluation results?

Response:

Good comment! It must be admitted that it is very important that both spatial and temporal scales of in-situ SSR measurements are commensurate with those of satellite retrievals. As pointed by Li et al. [2005], it incurs un-negligible errors to use instantaneous SSR measurements to validate coarse-resolution satellite retrievals. However, the spatial sampling uncertainties decrease rapidly as the time-averaging interval increases up to 24 h. Therefore, we compare the evaluation results of our SSR estimates with GLASS and ISCCP-FD product at a daily time scale. This information has been added in the text (L341-345) as “It may incur large errors to validate ISCCP-FD SSR products by using instantaneous in situ measurements because its spatial resolution is rather coarse (about 280 km). However, at daily time scale, the spatial sampling errors become small (Li et al., 2005). Thus, we compare our SSR estimates with GLASS and ISCCP-FD product at a daily time scale.”

Li, Z., Cribb, M., Chang, F. L., Trishchenko, A., and Luo, Y.: Natural variability and sampling errors in solar radiation measurements for model validation over the atmospheric radiation measurement Southern Great Plains region, *J. Geophys. Res.*, 110, D15S19, doi:10.1029/2004JD005028, 2005.

Minors:

Comment:

1. Page 35203, Line 13: “But their spatial resolutions (> 100 km) are too coarse to meet the requirements of land surface processes studies and practical applications.” I think it should be “But their spatial resolutions (> 100 km) are too coarse to meet the requirements of land surface processes studies and practical applications very well.”

Response:

Accepted!

Comment:

2. Page 35204, Line 23: “But it is difficult to directly derive cloud properties based on geostationary satellites due to their low spectral resolutions.” Quotations are needed for this expression.

Response:

The following three references have been added in the revised manuscript.

King, M. D., Tsay, S. C., Platnick, S. E., Wang, M. H., Liou, K. N.: Cloud retrieval algorithms for MODIS: optical thickness, effective particle radius, and thermodynamic phase, MODIS Algorithm Theoretical Basis Document No. ATBD-MOD-05, 1997.

Huang, J., Minnis, P., Lin, B., Yi, Y., Khaiyer, M., Arduini, R., Fan, A., and Mace, G.: Advanced retrievals of multilayered cloud properties using multispectral measurements, *J. Geophys. Res.*, 110, D15S18, doi:10.1029/2004JD005101, 2005.

Minnis, P., Huang, J., Lin, B., Yi, Y., Arduini, R., Fan, T., Ayers, J., and Mace, G.: Ice cloud properties in ice-over-water cloud systems using Tropical Rainfall Measuring Mission (TRMM) visible and infrared scanner and TRMM

Microwave Imager data, J. Geophys. Res., 112 (D6), D06206, doi:10.1029/2006JD007626, 2007.

Comment:

3. Page 35204, Line 23: I think “As well-known, the largest certainties....” should be “As well-known, the larger uncertainties ...”.

Response:

Compared with other factors such as aerosol, water vapor, ozone and so on, cloud actually is the largest uncertainty factor in satellite retrieval of SSR. Therefore, we think the “largest” is more proper than “larger”.

Comment:

4. Page 35205, Line 3: “MODIS and high temporal resolution radiance data of all MTSAT channels” should be “MODIS and high temporal resolution TOA radiance data of all MTSAT channels”.

Response:

Accepted!

Comment:

5. Page 35205, Line 3: I think the authors used to MTSAT-1R data. It should be described clearly here.

Response:

Yes, the observed SSR data in 2009 are used to validate the retrieved SSR, which were estimated from MTSAT-1R data. But, both MTSAT-1R and MTSAT-2 data are used in this study to map high spatio-temporal resolution SSR dataset (hourly, 5 km) over China from 2007 to 2014. We have added the information into the text (L103, L105-106).

Comment:

6. Page 35205, Line 20-25: Specific references should be included in the context.

Response:

The following two references have been added in the revised manuscript.

King, M., Menzel, W. P., Kaufman, Y. J., Tanre, D., Gao, B., Platnick, S., Ackerman, S. A., Remer, L. A., Pincus, R., Hubanks, P. K.: Cloud and aerosol properties, precipitable water, and profiles of temperature and water vapor from MODIS, IEEE T. Geosci. Remote, 41(2), 442–458, doi:10.1109/TGRS.2002.808226, 2003.

Schaaf, C.B., Gao, F., Strahler, A.H., Lucht, W., Li, X., Tsang, T., ... Roy, D.: First operational BRDF, albedo nadir reflectance products from MODIS, Remote Sens. Environ., 83, 135–148, doi:10.1016/S0034-4257(02)00091-3, 2002.

Retrieving high-resolution surface solar radiation with cloud parameters derived by combining MODIS and MTSAT data

W. Tang^{1,2,*}, J. Qin¹, K. Yang^{1,2}, S. Liu³, N. Lu⁴, X. Niu¹

1. Key Laboratory of Tibetan Environment Changes and Land Surface Processes, Institute of Tibetan Plateau Research, Chinese Academy of Sciences, Beijing 100101, China.
2. CAS Center for Excellence in Tibetan Plateau Earth Sciences, Chinese Academy of Sciences, Beijing 100101, China.
3. State Key Laboratory of Remote Sensing Science, School of Geography, Beijing Normal University, Beijing 100875, China.
4. State Key Laboratory of Resources and Environmental Information System, Institute of Geographic Sciences and Natural Resources Research, Chinese Academy of Sciences, Beijing 100101, China.

*Corresponding author and address:

Wenjun Tang, Dr.

Institute of Tibetan Plateau Research, Chinese Academy of Sciences

Building 3, Courtyard 16, Lin Cui Road, Chaoyang District, Beijing 100101, China

Email: tangwj@itpcas.ac.cn

1 **Abstract:** Cloud parameters (cloud mask, effective particle radius and liquid/ice
2 water path) are the important inputs in estimating surface solar radiation (SSR).
3 These parameters can be derived from MODIS with high accuracy but their temporal
4 resolution is too low to obtain high temporal resolution SSR retrievals. In order to
5 obtain hourly cloud parameters, the Artificial Neural Network (ANN) is applied in
6 this study to directly construct a functional relationship between MODIS cloud
7 products and Multi-functional Transport Satellite (MTSAT) geostationary satellite
8 signals. Meanwhile, an efficient parameterization model for SSR retrieval is
9 introduced and, when driven with MODIS atmospheric and land products, its root
10 mean square error (RMSE) is about 100 W m^{-2} for 44 Baseline Surface Radiation
11 Network (BSRN) stations. Once the estimated cloud parameters and other
12 information (such as aerosol, precipitable water, ozone and so on) are input to the
13 model, we can derive SSR at high spatio-temporal resolution. The retrieved SSR is
14 first evaluated against hourly radiation data at three experimental stations in the
15 Haihe River Basin of China. The mean bias error (MBE) and RMSE in hourly SSR
16 estimate are 12.0 W m^{-2} (or 3.5%) and 98.5 W m^{-2} (or 28.9%), respectively. The
17 retrieved SSR is also evaluated against daily radiation data at 90 China
18 Meteorological Administration (CMA) stations. The MBEs are 9.8 W m^{-2} (or 5.4%);
19 the RMSEs in daily and monthly-mean SSR estimates are 34.2 W m^{-2} (or 19.1%) and
20 22.1 W m^{-2} (or 12.3%), respectively. The accuracy is comparable or even higher than
21 other two radiation products (GLASS and ISCCP-FD), and the present method is
22 more computationally efficient and can produce hourly SSR data at a spatial

23 resolution of 5 km.

24

25 **Keywords:** Solar radiation; High resolution; Cloud parameters; Cloud detection

26 **1. Introduction**

27 Surface solar radiation (SSR), as a component of the surface radiation budget, is
28 the primary source of energy for the Earth's system. It controls both water and
29 energy exchanges on the land surfaces and thus is a major forcing for land surface
30 models, hydrological models, and ecological models (Xue et al., 2013; Huang et al.,
31 2016). SSR is also essential for many applications such as determination of the site
32 of solar power stations and design of heating systems (Berbery et al., 1999; Oliver
33 and Jackson, 2001; Roebeling et al., 2004; Mondol et al., 2008; Benghanem and
34 Mellit, 2010). However, *in situ* measurements of SSR are sparse, which are not
35 adequate to represent regional characteristics of SSR, due to high spatial variability
36 of SSR, especially in mountain regions.

37 Satellites can be utilized to retrieve spatially continuous SSR over a wide
38 geographical extent. Currently, there are several global satellite SSR products, such
39 as the Global Energy and Water cycle Experiment Surface Radiation Budget
40 (GEWEX-SRB, Stackhouse et al., et al., 2004,) and the International Satellite Cloud
41 Climatology Project Flux Data (ISCCP-FD, Zhang et al., 2004). But their spatial
42 resolutions (>100 km) are too coarse to **well** meet the requirements of land surface
43 processes studies and practical applications. Moreover, their accuracy needs further
44 improvements. As indicated by Yang et al. (2008), the SSR of GEWEX-SRB and
45 ISCCP-FD have large discrepancies in highly variable terrain in the Tibetan Plateau.
46 Wu et al. (2011) evaluated the monthly mean SSR of GEWEX-SRB over China, and
47 found that the SSR was generally overestimated over eastern China but occasionally

48 underestimated over western China. Therefore, it is necessary to develop new
49 methods that can produce high-accuracy and high-resolution SSR products.

50 So far, numerous methods have been developed to retrieve SSR from satellite
51 signals. These methods can be roughly divided into three categories. One is look-up
52 table methods that use satellite signals to match a pre-established radiative-transfer
53 database (Pinker et al., 2003; Liang et al., 2006; Mueller et al., 2009; Lu et al., 2010;
54 Huang et al., 2011; Ma and Pinker, 2012). These methods are not computational
55 economical, and most of them only use visible channel data. The second is
56 parameterization methods that directly calculate SSR by a parameterization model,
57 with **inputs** of cloud, aerosol and other atmospheric and surface variables (Zhang et
58 al., 2004; Halthore et al., 2005; Wang et al., 2009; Kim and Ramanathan, 2008;
59 Huang et al., 2012; Sun et al., 2012). Some inputs (e.g. cloud parameters) of these
60 methods change rapidly but it is hard to get **them with** high temporal resolution. The
61 third is statistical methods that directly link satellite-observed signals to SSR
62 measurements at regional scales (Lu et al., 2011). The disadvantage of these methods
63 is **their** limited generalization. In addition, the combination of the above methods is
64 also widely adopted by many researchers (e.g. Hammer et al., 2003; Rigollier et al.,
65 2004; Posselt et al., 2012; and Wang et al., 2011; 2014; Tanahashi et al., 2001;
66 Kawai and Kawamura, 2005; Yeom et al., 2008; 2010). These combined methods
67 firstly calculate clear-sky SSR by a look-up table method or a parameterization
68 method, and then the cloud index or cloud attenuation coefficient derived from
69 satellite data is used to calculate all-sky SSR. Their applicability needs further tests

70 at global scale.

71 Currently, both polar-orbit and geostationary satellites can be used to retrieve the
72 SSR, with different merits and defects. Sensors onboard polar-orbit satellites generally
73 have higher spectral resolutions than geostationary satellites. For example, the
74 Moderate Resolution Imaging Spectroradiometer (MODIS) onboard Terra and Aqua
75 platforms has 36 spectral bands, but the Multi-functional Transport Satellite (MTSAT)
76 and Geostationary Operational Environmental Satellites (GOES) have only five
77 spectral bands. Sensors with high spectral resolution have great advantage in
78 retrieving cloud properties (Huang et al., 2006). As a fact, MODIS can provide cloud
79 property data with high accuracy, which are used in many studies for SSR estimation
80 (Wang et al., 2009; Huang et al., 2011; Qin et al., 2015). However, their temporal
81 resolutions are too low to capture the diurnal cycle. By contrast, geostationary
82 satellites can provide continuous observations with high temporal resolutions, and
83 thus can capture the diurnal cycle of sky-conditions at regional scales. But it is
84 difficult to directly derive cloud properties based on geostationary satellites due to
85 their low spectral resolutions (King et al., 1997; Huang et al., 2005; Minnis et al.,
86 2007). As well-known, the largest uncertainties in satellite retrieval of SSR are
87 attributed to the inadequate information on cloud properties. Combination of
88 polar-orbit and geostationary satellites may provide an opportunity to derive the cloud
89 properties at high temporal resolutions.

90 This paper presents a new method to quickly estimate SSR by combining signals
91 of polar-orbit and geostationary satellites. This method includes two steps. The first

92 step is to estimate hourly cloud parameters by combining high-accuracy cloud
93 products of MODIS and high temporal resolution **top of atmosphere (TOA)** radiance
94 data of all MTSAT channels. The second step is to use the cloud information and
95 other auxiliary information in an efficient parameterization model to retrieve SSR at a
96 high spatio-temporal resolution. The paper is organized as follows. The data used are
97 introduced in Section 2. The SSR retrieval scheme is presented in Section 3. Section 4
98 presents the validation results and discussions. Finally, conclusions and remarks are
99 given in section 5.

100

101 **2 Data**

102 **2.1. MTSAT Data**

103 The MTSAT (**includes MTSAT-1R and MTSAT-2**) data of the Japan
104 Meteorological Agency (JMA) is used in this study. The MTSAT-1R, launched on 26
105 February 2005, is positioned at 140° E above the equator, and **the MTSAT-2, launched**
106 **on 18 February 2006, is positioned at 145° E above the equator.** As the next
107 generation of satellite series, they succeed the Geostationary Meteorological Satellite
108 (GMS) series and take over the role of observing East Asia and the Western Pacific.
109 The imager onboard MTSAT scans the earth every 30 minutes and provides images in
110 five channels (see Table 1). The spatial resolution of MTSAT data at nadir is 1 km for
111 the visible sensor, and 4 km for all the other infrared sensors. The visible and infrared
112 data were resampled to a spatial resolution of 5 km by Kochi University, and all these
113 five-channel data are used in this study to retrieve SSR.

114 2.2. MODIS Products

115 The MODIS level-2 products (version 5.1) are used in this study. These MODIS
116 products contains cloud products (MOD06, MYD06), aerosol products (MOD04,
117 MYD04), atmospheric profiles products (MOD07, MYD07), and albedo products
118 (MCD43C3), where MOD denotes data collected from the Terra platform, MYD
119 indicates data collected from Aqua platform, and MCD means combined product
120 derived from both Terra and Aqua platforms (Schaaf et al., 2002; King et al., 2003).
121 The spatial resolutions of the aerosol products (MOD04, MYD04), atmospheric
122 profiles products (MOD07, MYD07) and albedo products (MCD43C3) are 5 km;
123 whereas, the spatial resolution of cloud products is 1 km. Thus we resample the cloud
124 products to a spatial resolution of 5 km. The temporal resolution of atmosphere
125 products is generally two daytime observations every day, while that of MCD43C3 is
126 16 day.

127 These products are used for two purposes. One is to evaluate a new SSR retrieval
128 algorithm developed by the authors (Qin et al., 2015), which is driven by MODIS
129 atmospheric and land products. The inputs of this algorithm are MODIS products of
130 precipitable water, aerosol loading, ozone thickness, surface pressure, effective
131 particle radius of water/ice cloud, liquid/ice water path, cloud fraction, and ground
132 surface albedo. The other is to build mathematical relationships between MODIS
133 cloud products (effective particle radius and liquid/ice water path) and MTSAT
134 signals through ANN training, and then the cloud properties are estimated from
135 MTSAT signals by this ANN model. To reduce the uncertainty of the ANN model,

136 we only select high-quality MODIS data for the training.

137 **2.3. SSR Measurement Data**

138 Three types of surface radiation observation data are used to validate SSR
139 retrievals in this study. The first one is the ground measurements data collected at 44
140 Baseline Surface Radiation Network (BSRN) stations located in contrasting climatic
141 zones (see the Red Cross marks in Figure 1). Radiation observations at BSRN are
142 conducted with instruments of the highest available quality, and are recognized as the
143 most reliable data. Their temporal resolutions are 1 or 3 minutes. The measured SSR
144 are averaged over one hour centered on the satellite overpass. The second one is the
145 *in-situ* data collected at three experimental stations located in Haihe River Basin,
146 China. Figure 1 shows the spatial distribution of the experimental stations, which are
147 marked by the blue cross symbols, and the basic information on the three stations are
148 given in Table 2. The radiation data were sampled at every 1 or 2 s and the average
149 values of each 10 or 30 min were recorded. The detailed information about the
150 observations is available in Liu et al. (2013). The third one is the daily SSR data at
151 China Meteorological Administration (CMA) radiation stations. Figure 1 shows the
152 geographical distribution of these radiation stations denoted by circles throughout
153 China. The elevations of these stations vary from 1 to 4507 m. A set of quality-check
154 procedures has been applied to these data (Tang et al., 2010).

155

156 **3 SSR Retrieval Scheme**

157 The SSR retrieval scheme includes three key steps, as presented in Figure 2.

158 First, the clear-sky and cloudy conditions of the MTSAT data are flagged by cloud
159 detection in the image preprocessing procedure (Section 3.1), and the cloudy pixels
160 are divided into water cloud and ice cloud. Second, cloud parameters (effective
161 particle radius and liquid/ice water path) are derived by ANN models (Section 3.2)
162 built by all MTSAT channels signals and the MODIS level-2 cloud products. Third,
163 the hourly SSR is estimated by a physical retrieval algorithm (Section 3.3), given the
164 above derived cloud parameters and other inputs. Daily SSR values are obtained by
165 integrating hourly SSR values. The following three sub-sections describe the details
166 of each step.

167 **3.1 Cloud Detection**

168 Because of limitations of traditional cloud detection methods (e.g. threshold
169 approaches and statistical approaches) (Liu et al. 2009), an ANN method is trained
170 with the Levenberg-Marquardt optimization algorithm to detect clouds. Similar to
171 MODIS cloud mask, three classes (water cloud, ice cloud and clear land or sea) are
172 defined. The ANN contains three layers: input layer, output layer and one hidden
173 layer between them. The input layer has nine parameters, which are five MTSAT
174 channel signals, three angles information (the cosines of satellite viewing zenith
175 angle, solar zenith angle and the relative azimuth angle between the sun and the
176 satellite), and pixel's elevation. The hidden layer contains 20 neurons with
177 hyperbolic tangent sigmoid transfer function as the transfer function. In the output
178 layer, three neurons with linear transfer function are utilized to denote the cloud
179 detection results.

180 In the training, we select high-quality MODIS cloud mask data as the “truth” of
181 the output, and the MTSAT signals as input. To enhance the possibility of
182 distinguishing clouds from snow, we also randomly choose clear-sky pixels above
183 snow surface and cloud-sky pixels above snow surface through visual identification.
184 Finally, the trained ANN is used to detect clouds, and the result is one of clear sky,
185 water cloud and ice cloud.

186 One may question that the trained ANN may lose representativeness for cases
187 that solar zenith angles are large (e.g., the hours around sunrise and sunset), because
188 the overpass times of Terra-MODIS and Aqua-MODIS roughly are 10:30 and 13:30,
189 around which the solar zenith angles are relatively small. To alleviate this issue, a
190 large number of data points are selected in this study to train the ANN. These data
191 points cover most of China and span all four seasons. We have checked the training
192 data and found that the values of solar zenith angle vary from about 7.1° to 78.3° .
193 This range of solar zenith angle is sufficiently wide except for extreme cases such as
194 the hours around sunrise and sunset, but the value of SSR is very small in the
195 extreme cases. Also, it should be noted that the angle information is not the
196 determinative factor in cloud detection.

197 **3.2 Cloud Parameter Estimation**

198 Similar to Section 3.1, another ANN model is used to estimate cloud parameters
199 (effective particle radius and liquid/ice water path) from MTSAT image. Again, the
200 ANN model is trained with high-quality MODIS cloud products as “truth” of the
201 output and MTSAT signals as input. The MODIS cloud products are randomly

202 selected, and split into two parts: one for training and other for independent
203 validation. Comparison between the two parts indicates that the trained ANNs
204 behave similar to each other. To improve the generalization of the ANN model, we
205 use all the data to train the ANN.

206 **After all the data are used to train the ANN,** Figures 3 and 4 show the cloud
207 parameters (effective particle radius and liquid/ ice water path) comparisons between
208 the MODIS “true values” and the estimated ones by ANNs for water cloud and ice
209 cloud, respectively. It can be seen that the estimated effective particle radius for both
210 water cloud and ice cloud are generally comparable to the observed ones, and their
211 correlation coefficients are both greater than 0.60. The estimated liquid/ice water
212 path for both water cloud and ice cloud are generally consistent with the observed
213 ones, and their correlation coefficients are both greater than 0.70. The performance
214 of the trained ANNs for both water cloud and ice cloud at other pixels, which are not
215 used to build the ANNs, behaves similar as to the ones in Figures 3 and 4 (not shown
216 here). Therefore, the built ANNs can catch the functional relationships between the
217 MODIS cloud parameters and MTSAT signals. Based on the ANNs, the cloud
218 parameters can be efficiently derived from MTSAT data for the estimation of high
219 spatio-temporal resolution SSR.

220 **To further investigate the effect of errors in cloud parameters estimates on the**
221 **accuracy of the SSR retrieval algorithm, a sensitivity test of the SSR retrieval**
222 **algorithm to cloud parameters (effective particle radius and liquid/ice water path) is**
223 **presented in Figure 5. The condition used for the sensitivity test is specified as a**

224 mid-latitude atmosphere with: solar zenith angle of 60 degree, surface elevation of 0.0
225 km, precipitable water of 0.14 cm, total ozone amount of 0.25 cm, surface albedo of 0.2
226 and Ångström turbidity coefficient of 0.1. We estimated the sensitivity of SSR
227 retrieval to estimation errors in both liquid/ice water path and effective particle radius.
228 As shown in Figure 3 and Figure 4, the estimated mean effective particle radius within
229 one standard deviation (1σ) correspond to the ranges of about 8-12 μm and 22-30 μm
230 for water cloud and ice cloud, which would lead to SSR changing about 25 W m^{-2} and
231 15 W m^{-2} as seen from Figure 5, respectively. The estimated mean cloud liquid/ice
232 water path within 1σ correspond to the ranges of about 45-185 g m^{-2} , 80-240 g m^{-2} ,
233 which would lead to SSR changing about 154 W m^{-2} and 172 W m^{-2} , respectively.
234 Obviously, errors in SSR caused by the cloud liquid/ice water path estimation errors
235 are much greater than the ones caused by cloud effective particle estimation errors.

236 3.3 SSR Retrieval Algorithm

237 The SSR retrieval algorithm used in this study is developed by Qin et al. (2015).
238 This algorithm is mainly based on the cloud parameterization developed by Chou et al.
239 (1999) and a clear-sky broadband radiative transfer model developed by Yang et al.
240 (2006). The detailed description of cloud parameterization and the SSR
241 parameterization are presented in Appendix A1 and A2, respectively.

242 In order to estimate the SSR, the retrieval algorithm needs to input cloud
243 parameters, surface elevation, the precipitable water (PW), the thickness of ozone
244 layer, the Ångström turbidity coefficient, and surface albedo. Qin et al. (2015) drove
245 the algorithm with MODIS level-2 atmospheric and land products and validated the

246 instantaneous SSR at nine stations. The mean Root Mean Square Error (RMSE) is
247 about 100 W m^{-2} . To further test the performance of the algorithm globally, we
248 validated the instantaneous SSR estimated with MODIS products at 44 BSRN
249 stations in 2009. Figure 6 presents validation results. The mean RMSEs for Terra and
250 Aqua are about 101 W m^{-2} and 106 W m^{-2} , which may indicate that this algorithm
251 can effectively retrieve SSR based on MODIS products globally. Therefore, we may
252 expect to apply the algorithm on the geostationary satellite.

253 The key of applying the SSR retrieval algorithm on geostationary satellite is the
254 acquisition of input parameters. The cloud parameters can be derived efficiently by
255 the ANNs in sub-section 3.2. The influence of the PW on the SSR is significant for
256 the cloud-free conditions. Therefore, the PW here is derived by the split-window
257 algorithm of Chesters et al., (1987) under cloud-free conditions as adopted by
258 Tanahashi et al., (2001) and Lu et al., (2010). However, the PW for cloudy
259 conditions is set at 2.9 g/cm^2 , as defined in the standard atmospheric profile of the
260 mid-latitude summer model, since the cloud effects on the SSR is dominant. The
261 Ångström turbidity coefficient is produced by the GADS (Global Aerosol Data Set
262 2.2a; see Koepke et al., 1997 and Hess et al., 1998) model. The thickness of ozone
263 layer is obtained from TOMS (Total Ozone Mapping Spectrometer) zonal means
264 provided by NASA/GSFC Ozone Processing Team (see
265 <https://ozoneaq.gsfc.nasa.gov/data/toms/>). The surface elevation data are from the
266 near-global elevation model Shuttle Radar Topography Mission (SRTM) 30 data set
267 and have been averaged to the 0.05° latitude-longitude grids of the MTSAT imagery.

268 The surface albedo data are from the MODIS MCD43A3 16 day albedo.

269 **4 Results and Discussions**

270 As mentioned above, SSR measurements at three experimental stations over
271 Haihe River Basin and 90 CMA radiation stations in 2009 are used to evaluate the
272 accuracy of the hourly, daily and monthly SSR retrieval from collocated satellite
273 pixels, respectively. The performance of the SSR estimate is evaluated using three
274 metrics: mean bias error (MBE, in $W m^{-2}$), RMSE, (in $W m^{-2}$), and correlation
275 coefficient (R).

276 **4.1 Validation of Hourly SSR in Haihe River Basin**

277 Pinker et al. (2003) pointed out that an hourly interval is suitable for evaluating
278 satellite instantaneous SSR retrievals due to the dependence on the average speed of
279 cloud movement. Furthermore, Deneke et al. (2009) demonstrated that the observed
280 SSR averaging over a period of 40-80 min is optimal for a comparison with satellite
281 retrievals. Therefore, here we adopt hourly SSR observations, centered on the time
282 of the satellite overpass on the hour, to evaluate the satellite-derived hourly values.
283 Figures 7(a)-(c) show the validation results of the hourly SSR estimates in 2009 at
284 the three experimental stations (Miyun, Daxing, and Guantao) in Haihe River Basin.
285 The average RMSE on an hourly timescale for these three stations is $98.5 W m^{-2}$
286 (28.9%) and the corresponding MBE is $12.0 W m^{-2}$ (3.5%). The overall positive
287 MBE indicates overestimation of the hourly SSR retrievals with MTSAT data at the
288 three stations. **The lack of three-dimensional radiative effects in the SSR retrieval**

289 algorithm and the appearance of broken clouds are the potential reasons for the
290 hourly SSR bias (Deneke et al., 2008). Another reason for the discrepancies may be
291 attributed to the different amounts of cloud in the different illumination and viewing
292 paths when comparing the satellite retrievals with the ground measurements (Liang
293 et al., 2006). In addition, it might be caused by the retrieval algorithm error.

294 In a word, although the retrievals in Haihe River Basin have slight biases
295 toward overestimating the hourly SSR values, the results still indicate acceptable
296 agreement between satellite retrievals and ground observations at the hourly time
297 scale.

298 **4.2 Validation of Daily and Monthly SSR at CMA**

299 Figure 8 shows the validation results for the daily and monthly mean SSR
300 estimates at all CMA radiation stations, respectively. The daily and monthly mean
301 SSR estimates show high correlation with the ground SSR measurements, with
302 correlation coefficients of 0.93 and 0.95, respectively. Both the daily and monthly
303 mean SSR estimates exhibit a positive mean bias of 9.8 W m^{-2} (or 5.4%) and RMSE
304 of 34.2 W m^{-2} (or 19.1%) on daily scale, 22.1 W m^{-2} (or 12.3%) on monthly scale.
305 These RMSE values are comparable to the results of Kawai and Kawamura (2005)
306 with 19.5% daily RMSE, those of Lu et al. (2010) with 17.7% daily RMSE, and the
307 results of Lu et al. (2011) with 20.4% daily RMSE and 11.4% monthly RMSE.
308 Moreover, the daily mean RMSE of our study is obviously lower than that of Jia et al.
309 (2013), which estimates SSR with FY-2C and their daily mean RMSE over China is
310 about 49.3 W m^{-2} (or 27.5%). These results suggest that our SSR estimation with

311 MTSAT data works well for various climate regions, land cover types and elevations.
312 The differences between satellite-derived estimates and ground observations may be
313 attributed to calibration uncertainty of the satellite sensor, the cloud detection error,
314 uncertainty in the retrieval algorithm, errors in ground observations, and the
315 representativeness of the station data. The representativeness of the station data is
316 crucial for evaluating the satellite-derived estimates. For example, the Ermeishan
317 station (No. 56385) of CMA was deployed at the top of Emei Mountain, which
318 cannot well represent the corresponding pixel of MTSAT. The mean elevation of the
319 pixel is 1005 m, while the station's elevation is 3047 m.

320 The spatial distribution of MBE and RMSE for daily and monthly mean SSR
321 estimates at all the CMA radiation stations are presented in Figure 9, respectively.
322 Most of daily and monthly mean MBE values are positive and less than 30 W m^{-2} .
323 The large positive MBE mainly located in the southern China, in which the
324 corresponding RMSE values are relatively large. This phenomenon can be easily
325 explained. Because southern China (20° - 35° N, 103° - 120° E) is the largest cloudy
326 subtropical continental region (Yu et al. 2001), which was also confirmed by Li et al.
327 (2004) based on multi-year ISCCP data and surface cloud observations. When cloud
328 distribution become more complicated, the accuracy of cloud parameters estimates
329 (see section 3.3) would decrease, and leads to larger error in SSR retrieval. However,
330 most of the RMSEs are less than 40 W m^{-2} for daily SSR and less than 30 W m^{-2} for
331 monthly mean SSR, indicating the retrieval algorithm had relatively reliable
332 estimation performance at individual observation station.

333 4.3 Comparisons with Other SSR Estimates

334 Two satellite SSR products are selected to compare with the SSR estimate in this
335 study. One is the Global Land Surface Satellite (GLASS) SSR products, which were
336 also retrieved from MTSAT data by look-up table method (Zhang et al. 2014). The
337 GLASS SSR algorithm is similar to the photosynthetically active radiation (PAR)
338 retrieval algorithm of Liang et al. (2006). The other is the ISCCP-FD SSR products,
339 which were produced by a NASA Goddard Institute for Space Studies (GISS)
340 radiative transfer model based on the ISCCP D1 data at 2.5° spatial resolution and
341 3-hour temporal resolution (Zhang et al., 2004). It may incur large errors to validate
342 ISCCP-FD SSR products by using instantaneous in situ measurements because its
343 spatial resolution is rather coarse (about 280 km). However, at daily time scale, the
344 spatial sampling errors become small (Li et al., 2005). Thus, we compare our SSR
345 estimates with GLASS and ISCCP-FD product at a daily time scale. Figure 10 shows
346 the performance comparisons between our SSR estimates and the two satellites SSR
347 products on a daily time scale at all CMA radiation stations except the Ermeishan
348 station during 2009. The number of daily validation data here is less than the one in
349 Figure 7(a) due to some missing values in the GLASS products at some points, which
350 are excluded from comparison. As shown in the Figure 10, the ISCCP-FD SSR
351 retrievals perform slightly worse than the ones of our algorithm and the GLASS in
352 terms of RMSE and R. The RMSE of our algorithm is comparable to the one of
353 GLASS, though the MBE of our algorithm is larger than the one of GLASS. The
354 GLASS produces smaller scattering than our algorithm, while it underestimates the

355 SSR at peak values and overestimates the SSR at low values. This would be due to the
356 coarse spectral resolution of geostationary satellites (MTSAT), which cannot work
357 well in the extreme conditions (namely, extremely low value and high value). Another
358 feature is that our algorithm generally overestimates the SSR, with mean MBE of 9.4
359 W m^{-2} . This phenomenon may be attributed to the general underestimations of liquid
360 water path and ice water path, which can be seen in Figures 3 and 4. We suspect that
361 the general underestimations of liquid water path and ice water path in Figures 3 and 4
362 would also stem from the coarse spectral resolution of MTSAT. However, the linear
363 fitting curve of our estimate is closer to the 1:1 line than the ones of the GLASS and
364 the ISCCP-FD. This demonstrates that our algorithm can produce a comparable or
365 even higher accuracy than the GLASS and the ISCCP-FD products.

366 **4.4 Applications in China**

367 Based on the above SSR retrieval scheme and MTSAT data, we derive an
368 eight-year high spatio-temporal resolution SSR dataset (hourly, 5 km) over China
369 from 2007 to 2014. This dataset is significantly important for the regions where few
370 ground-based measurements are available, such as the Tibetan Plateau. Figure 11
371 shows the monthly-mean SSR images for 12 months in 2009 over the mainland
372 China. As seen, these 12 images thoroughly exhibit the spatial-temporal patterns of
373 SSR over the mainland China. The spatial distribution characteristics of Figure 11
374 are consistent with the result of Tang et al. (2013), which was derived based on the
375 SSR estimations at 716 CMA stations. The SSR values are the highest in summer
376 and lowest in winter, spring and autumn are in the midst. The formation of this

377 phenomenon is primarily controlled by sun elevation and the annual cycle of day
378 length. In addition, some interesting regional characteristics can be found. The
379 maximum radiation appears over the Tibetan Plateau, where the average elevation is
380 more than 4 km and thus radiation extinction is small. The minimum radiation is
381 over southwestern China (Sichuan Basin and Guizhou), where are often covered by
382 stratiform clouds. Meanwhile, both the two extreme values lie on the belt between
383 25°N and 35°N. SSR generally increases from east to west except for southwestern
384 China, and decreases with increasing latitude in the western China. There is no doubt
385 that the sparse ground-based observations could not distinguish such regional
386 differences in SSR distribution. The eight-year SSR dataset will be released after the
387 publication of this article.

388

389 **5 Conclusions and Remarks**

390 To obtain high-resolution SSR data, this study developed an ANN-based
391 algorithm to estimate cloud parameters (cloud mask, effective particle radius and
392 liquid/ice water path) from MTSAT imagery. The algorithm was built by the
393 combination of MODIS cloud products and MTSAT data. The estimated cloud
394 parameters and other information (such as aerosol, ozone, PW and so on) were put
395 into a parameterization model to estimate SSR. The estimated SSR was validated
396 against both experimental data and operational station data in China, with RMSE of
397 98.5 W m⁻² for hourly SSR, 34.2 W m⁻² for daily SSR and 22.1 W m⁻² for monthly
398 SSR, and MBE of about 10 W m⁻².

399 Compared with two satellite radiation products (GLASS and ISCCP-FD), the
400 SSR estimate presented in this study has a comparable accuracy in terms of RMSE.
401 The GLASS underestimates the peak values of SSR while overestimates the low
402 values. Our algorithm generally overestimates the SSR, which might be attributed to
403 the underestimation of the cloud water path. The combining of CLOUDSAT and
404 MTSAT in the future may be an alternative method to further improve the accuracy
405 of cloud parameters, because the CLOUDSAT has more advantage in retrieving
406 cloud parameters than MODIS.

407

408 **Appendix A**

409 **A.1 Cloud Parameterization**

410 The cloud parameterization schemes of Chou et al. (1999) are actually
411 parameterization of three key parameters, which are optical thickness,
412 single-scattering co-albedo and asymmetry factor, for ice/water cloud at 11
413 individual broad spectral bands, respectively. They are expressed as:

$$414 \quad \delta = CWP(a_0 + a_1/r_e), \quad (\text{A1})$$

$$415 \quad 1 - \omega = b_0 + b_1 r_e + b_2 r_e^2, \quad (\text{A2})$$

$$416 \quad g = c_0 + c_1 r_e + c_2 r_e^2, \quad (\text{A3})$$

417 where a , b , and c are regression coefficients and their values are given in Chou et al.
418 (1999). r_e is the effective particle radius for ice/water cloud, and CWP is the cloud
419 ice/water path. Taking the ratio of the extraterrestrial solar radiation of each band to
420 that of the total spectrum for weight, thus the single-scattering properties for

421 ice/water cloud at shortwave broadband can be derived, respectively.

$$422 \quad \bar{\delta} = -\log \left(\frac{\sum_{i=1}^{11} S_{0i} * e^{(-\delta_i)}}{\sum_{i=1}^{11} S_{0i}} \right), \quad (\text{A4})$$

$$423 \quad \bar{\omega} = -\log \left(\frac{\sum_{i=1}^{11} S_{0i} * e^{(-\delta_i * \omega_i)}}{\sum_{i=1}^{11} S_{0i}} \right) / \bar{\delta}, \quad (\text{A5})$$

$$424 \quad \bar{g} = -\log \left(\frac{\sum_{i=1}^{11} S_{0i} * e^{(-\delta_i * \omega_i * g_i)}}{\sum_{i=1}^{11} S_{0i}} \right) / (\bar{\delta} * \bar{\omega}), \quad (\text{A6})$$

425 where δ_i , ω_i and g_i are the single-scattering properties for ice/water cloud at each
 426 band, S_{0i} is the extraterrestrial solar radiation of each band.

427 Therefore, if the values of *CWP* and *re* were known, the single-scattering
 428 properties at shortwave broadband can be determined. Furthermore, the
 429 transmittance due to water cloud attenuation ($\bar{\tau}_{wc}$) and ice cloud attenuation ($\bar{\tau}_{ic}$)
 430 can be obtained as follow,

$$431 \quad \bar{\tau}_{wc} = e^{(-\bar{\delta}_w / \mu_0)}, \quad (\text{A7})$$

$$432 \quad \bar{\tau}_{ic} = e^{(-\bar{\delta}_i / \mu_0)}, \quad (\text{A8})$$

433 where μ_0 is the cosine of solar zenith angle. $\bar{\tau}_{wc}$ and $\bar{\tau}_{ic}$ can be divided into
 434 processes of scattering and absorption, respectively.

$$435 \quad \bar{\tau}_{wc} = \bar{\tau}_{wca} \bar{\tau}_{wcs}, \quad (\text{A9})$$

$$436 \quad \bar{\tau}_{ic} = \bar{\tau}_{ica} \bar{\tau}_{ics}, \quad (\text{A10})$$

437 where $\bar{\tau}_{wca}$ And $\bar{\tau}_{wcs}$ are transmittances due to water cloud absorption and

438 scattering, respectively; $\bar{\tau}_{ica}$ and $\bar{\tau}_{ics}$ are transmittances due to ice cloud absorption
 439 and scattering, respectively.

440 A.2 SSR Parameterization

441 SSR under cloudy sky conditions can be given by the following equation, if not
 442 taking into account the multiple reflections between the ground and atmosphere,

$$443 R_{sw,clد} = R_0(\bar{\tau}_b + \bar{\tau}_d), \quad (A11)$$

444 where R_0 is solar radiation on a horizontal surface at the top of atmosphere, $\bar{\tau}_b$ and
 445 $\bar{\tau}_d$ are the broadband direct radiative transmittance and the diffuse radiative
 446 transmittance, which are given by,

$$447 \bar{\tau}_b \approx \bar{\tau}_{oz} \bar{\tau}_w \bar{\tau}_g \bar{\tau}_r \bar{\tau}_a \bar{\tau}_c, \quad (A12)$$

$$448 \bar{\tau}_d = \bar{\tau}_{d1} + \bar{\tau}_{d2} + \bar{\tau}_{d3}, \quad (A13)$$

449 where $\bar{\tau}_r$, $\bar{\tau}_a$, $\bar{\tau}_{oz}$, $\bar{\tau}_w$, $\bar{\tau}_g$ and $\bar{\tau}_c$ are, respectively, solar radiation
 450 transmittances of six damping processes in the atmospheric layer, viz. Rayleigh
 451 scattering, aerosol extinction, ozone absorption, water vapor absorption, permanent
 452 gases absorption and cloud extinction. $\bar{\tau}_a$ is divided into processes of scattering
 453 and absorption.

$$454 \bar{\tau}_a = \bar{\tau}_{aa} \bar{\tau}_{as}, \quad (A14)$$

455 where $\bar{\tau}_{aa}$ and $\bar{\tau}_{as}$ are transmittances due to the aerosol absorption and scattering,
 456 respectively. The detailed calculation of $\bar{\tau}_r$, $\bar{\tau}_a$, $\bar{\tau}_{oz}$, $\bar{\tau}_w$ and $\bar{\tau}_g$ can be found in
 457 Yang et al. (2006). $\bar{\tau}_c$ can be calculated according the above cloud
 458 parameterization scheme.

459 $\bar{\tau}_{d1}$, $\bar{\tau}_{d2}$ and $\bar{\tau}_{d3}$ are forward diffuse radiative transmittances due to Rayleigh
 460 scattering, aerosol scattering, cloud scattering, and are given by,

$$461 \quad \bar{\tau}_{d1} \approx 0.5 \bar{\tau}_{oz} \bar{\tau}_g \bar{\tau}_w \bar{\tau}_{aa} \bar{\tau}_{wca} (1 - \bar{\tau}_r) \quad \text{for water cloud,} \quad (\text{A15a})$$

$$462 \quad \bar{\tau}_{d1} \approx 0.5 \bar{\tau}_{oz} \bar{\tau}_g \bar{\tau}_w \bar{\tau}_{aa} \bar{\tau}_{ica} (1 - \bar{\tau}_r) \quad \text{for ice cloud,} \quad (\text{A15b})$$

$$463 \quad \bar{\tau}_{d2} \approx f_a(\mu_0) \bar{\tau}_{oz} \bar{\tau}_g \bar{\tau}_w \bar{\tau}_{aa} \bar{\tau}_{wca} \bar{\tau}_r (1 - \bar{\tau}_{as}) \quad \text{for water cloud,} \quad (\text{A16a})$$

$$464 \quad \bar{\tau}_{d2} \approx f_a(\mu_0) \bar{\tau}_{oz} \bar{\tau}_g \bar{\tau}_w \bar{\tau}_{aa} \bar{\tau}_{ica} \bar{\tau}_r (1 - \bar{\tau}_{as}) \quad \text{for ice cloud,} \quad (\text{A16b})$$

$$465 \quad \bar{\tau}_{d3} \approx f_w(\mu_0) \bar{\tau}_{oz} \bar{\tau}_g \bar{\tau}_w \bar{\tau}_{aa} \bar{\tau}_{wca} \bar{\tau}_r \bar{\tau}_{as} (1 - \bar{\tau}_{wcs}) \quad \text{for water cloud,} \quad (\text{A17a})$$

$$466 \quad \bar{\tau}_{d3} \approx f_i(\mu_0) \bar{\tau}_{oz} \bar{\tau}_g \bar{\tau}_w \bar{\tau}_{aa} \bar{\tau}_{ica} \bar{\tau}_r \bar{\tau}_{as} (1 - \bar{\tau}_{ics}) \quad \text{for ice cloud,} \quad (\text{A17b})$$

467 where 0.5 is the fraction of the Rayleigh-scattered flux which is scattered into the
 468 downward hemisphere (another 0.5 is scattered upward). $f_a(\mu_0)$ is the fraction of
 469 the aerosol-scattered flux which is scattered into the downward hemisphere
 470 ($1 - f_a(\mu_0)$ is scattered upward), $f_w(\mu_0)$ is the fraction of the water cloud-scattered
 471 flux which is scattered into the downward hemisphere ($1 - f_w(\mu_0)$ is scattered
 472 upward), $f_i(\mu_0)$ is the fraction of the ice cloud-scattered flux which is scattered into
 473 the downward hemisphere ($1 - f_i(\mu_0)$ is scattered upward). The factors $f_a(\mu_0)$,
 474 $f_w(\mu_0)$ and $f_i(\mu_0)$, which depend on cosine of the solar zenith angle (μ_0) and the
 475 asymmetry factor (g) and can be derived by integration of scattering phase function,
 476 are given according to parameterization of P. räisänen (2002) by,

$$477 \quad f_a(\mu_0) = 0.4482 + (5.3664 - 22.1608t + 28.6995t^2 - 11.1348t^3) \left(\frac{g_a}{g_a + 1} \right), \quad (\text{A18a})$$

$$478 \quad f_w(\mu_0) = 0.3312 + 1.1285(\mu_0^{0.7469}) \left(\frac{g_w}{g_w + 1} \right), \quad (\text{A18b})$$

479 $f_i(\mu_0) = 0.4250 + 0.9595(\mu_0^{0.8484})\left(\frac{g_i}{g_i + 1}\right),$ (A18c)

480 $t = (\mu_0 + 0.1)^{0.25},$ (A19)

481 where, g_a, g_w and g_i are the asymmetry factors of aerosol, water cloud, and ice
 482 cloud, respectively. The asymmetry factors of water cloud and ice cloud can be
 483 calculated according the above cloud parameterization. While the asymmetry factors
 484 and single-scattering albedo of the aerosol are interpolated from the observed ones at
 485 all the AEROSOL ROBOTIC NETWORK (AERONET) sites (Dubovik and King, 2000).

486 Considering the multiple reflections between the ground and atmosphere, The
 487 SSR can be given by,

488
$$R_{sw} = \frac{(1 - C_w - C_i)R_{sw,clr} + C_w R_{sw,wc} + C_i R_{sw,ic}}{(1 - \rho_{a,all}\rho_g)},$$

489 (A20)

490 where R_{sw} is SSR, C_w and C_i are water cloud cover and ice cloud cover,
 491 respectively. $R_{sw,clr}$, $R_{sw,wc}$ and $R_{sw,ic}$ are SSR under clear-sky, water cloudy sky
 492 and ice cloudy sky, respectively. $R_{sw,clr}$ can be derived from equations (11-17)
 493 when $\bar{\tau}_c, \bar{\tau}_{wca}, \bar{\tau}_{ica}, \bar{\tau}_{wcs}, \bar{\tau}_{ics}$ are all equal to 1. $\rho_{a,all}$ and ρ_g are albedos of
 494 atmospheric and ground, respectively. $\rho_{a,all}$ can be determined by,

495 $\rho_{a,all} = (1 - C_w - C_i)\rho_{a,clr} + C_w \rho_{a,wc} + C_i \rho_{a,ic},$ (A21)

496 where $\rho_{a,clr}$, $\rho_{a,wc}$ and $\rho_{a,ic}$ are albedos of atmospheric under clear sky, water cloudy
 497 sky and ice cloudy sky, respectively. They are given by

498 $\rho_{a,clr} \approx \bar{\tau}'_g \bar{\tau}'_w \bar{\tau}'_{oz} \bar{\tau}'_{aa} \{0.5(1 - \bar{\tau}'_r) + [1 - f_a(1/\sqrt{3})]\bar{\tau}'_r(1 - \bar{\tau}'_{as})\}$

499 for clear skies, (A22a)

500 $\rho_{a,wc} \approx \bar{\tau}'_g \bar{\tau}'_w \bar{\tau}'_{oz} \bar{\tau}'_{aa} \bar{\tau}'_{wca} \{0.5(1 - \bar{\tau}'_r) + [1 - f'_a(1/\sqrt{3})] \bar{\tau}'_r (1 - \bar{\tau}'_{as}) + [1 - f'_w(1/\sqrt{3})] \bar{\tau}'_r \bar{\tau}'_{as} (1 - \bar{\tau}'_{wcs})\}$
 501 for water cloud, (A22b)

502 $\rho_{a,ic} \approx \bar{\tau}'_g \bar{\tau}'_w \bar{\tau}'_{oz} \bar{\tau}'_{aa} \bar{\tau}'_{ica} \{0.5(1 - \bar{\tau}'_r) + [1 - f'_a(1/\sqrt{3})] \bar{\tau}'_r (1 - \bar{\tau}'_{as}) + [1 - f'_i(1/\sqrt{3})] \bar{\tau}'_r \bar{\tau}'_{as} (1 - \bar{\tau}'_{ics})\}$
 503 for ice cloud, (A22c)

504 where the transmissivities $\bar{\tau}'_g, \bar{\tau}'_w, \bar{\tau}'_{oz}, \bar{\tau}'_r, \bar{\tau}'_{aa}, \bar{\tau}'_{as}, \bar{\tau}'_{wca}, \bar{\tau}'_{ica}, \bar{\tau}'_{ics}$ and $\bar{\tau}'_{ics}$ are all
 505 evaluated at an effective relative air mass of $\sqrt{3}$ to account for absorption or
 506 reflectance over path lengths averaged over the whole upward hemisphere.

507

508 **Acknowledgments**

509 This work was supported by the National Natural Science Foundation of China
 510 (Grant No. 41301359), "Strategic Priority Research Program (B)" of the Chinese
 511 Academy of Sciences (Grant No. XDB03030306), National Natural Science
 512 Foundation of China (Grant No. 41190083; 41325019), Open Fund from the State
 513 Key Laboratory of Remote Sensing Science (grant OFSLRSS201303) that is
 514 cosponsored by the Institute of Remote Sensing and Digital Earth, Chinese Academy
 515 of Sciences and Beijing Normal University. CMA radiation data were obtained from
 516 the National Meteorological Information Center. MTSAT data is available via the
 517 website (<http://weather.is.kochi-u.ac.jp/sat/GAME/>). MODIS data is available via
 518 the website (<http://reverb.echo.nasa.gov/reverb/>). BSRN radiation data is available
 519 via the website (<http://www.bsrn.awi.de>). GLASS radiation data is available via the
 520 website (<http://glass-product.bnu.edu.cn/>). ISCCP-FD radiation data is available via
 521 the website (<http://isccp.giss.nasa.gov>).

522 **References**

- 523 Benghanem M, Mellit A.: Radial basis function network-based prediction of global
524 solar radiation data: application for sizing of a stand-alone photovoltaic system
525 at Al-Madinah, Saudi Arabia, *Energy*, 35, 3751–3762, 2010.
- 526 Berbery, E. H., Mitchell, K. E., Benjamin, S., Smirnova, T., Ritchie, H., Hogue, R.,
527 and Radeva, E.: Assessment of land-surface energy budgets from regional and
528 global models, *J. Geophys. Res.*, 104, 19329–19348, 1999.
- 529 Chesters, D., Robinson, W. D. and Uccellini, L. W.: Optimized retrievals of
530 precipitable water from the VAS “Split Windows”, *J. Clim. Appl. Meteorol.*, 26,
531 10591066, doi:10.1175/1520-0450(1987)026<1059:OROPWF>2.0.CO;2, 1987.
- 532 Chou, M.-D. and Suarez, M. J.: A Solar Radiation Parameterization for Atmospheric
533 Studies, NASA Tech. Rep. Ser. Global Model. Data Assimilation, vol. 15,
534 NASA Tech. Memo., TM-1999-104606, Maryland, USA, 42 pp., 1999.
- 535 Deneke, H., Feijt, A. and Roebeling R.: Estimating surface solar irradiance from
536 METEOSAT SEVIRI-derived cloud properties, *Remote Sens. Environ.*, 112,
537 3131-3141, doi:10.1016/j.rse.2008.03.012, 2008.
- 538 Deneke, H. M., Knap, W. H. and Simmer C.: Multiresolution analysis of the
539 temporal variance and correlation of transmittance and reflectance of an
540 atmospheric column, *J. Geophys. Res.*, 114, D17206,
541 doi:10.1029/2008JD011680, 2009.
- 542 Dubovik, O. and King M. D.: A flexible inversion algorithm for retrieval of aerosol
543 optical properties from Sun and sky radiance measurements, *J. Geophys.*

544 Res., 105, 20673-20696, 2000.

545 Hammer, A., Heinemann, D., Hoyer, C., Lorenz, E., Muller, R., and Beyer, H. G.:
546 Solar energy assessment using remote sensing technologies, *Remote Sens.*
547 *Environ.*, 86(3), 423–432, doi:10.1016/S0034-4257(03)00083-X, 2003.

548 Halthore, R. N., Crisp, D., Schwartz, S. E., Anderson, G. P., Berk, A., Bonnel, B.,
549 Boucher, O., Chang, F.-L., Chou, M.-D., Clothiaux, E. E., Dubuisson, P., Fomin,
550 B., Fouquart, Y., Freidenreich, S., Gautier, C., Kato, S., Laszlo, I., Li, Z.,
551 Mather, J. H., Plana-Fattori, A., Ramaswamy, V., Ricchiazzi, P., Shiren, Y.,
552 Trishchenko, A., and W. Wiscombe: Intercomparison of shortwave radiative
553 transfer codes and measurements, *J. Geophys. Res.*, 110, D11206,
554 doi:10.1029/2004JD005293, 2005.

555 Hess, M., Koepke, P., Schult, I.: Optical properties of aerosol and clouds: the
556 software package OPAC, *B. Am. Meteorol. Soc.*, 79, 831–844, 1998.

557 Huang, G., Ma, M., Liang, S., Liu, S., and Li, X.: A LUT-based approach to estimate
558 surface solar irradiance by combining MODIS and MTSAT data, *J. Geophys.*
559 *Res.*, 116, D22201, doi:10.1029/2011JD016120, 2011.

560 Huang G., Liu S., Liang S.: Estimation of net surface shortwave radiation from
561 MODIS data, *Int. J. Remote Sens.*, 33(3), 804–825, 2012.

562 Huang, J., Minnis, P., Lin, B., Yi, Y., Khaiyer, M., Arduini, R., Fan, A., and Mace, G.:
563 Advanced retrievals of multilayered cloud properties using multispectral
564 measurements, *J. Geophys. Res.*, 110, D15S18, doi:10.1029/2004JD005101,
565 2005.

566 Huang, J., Minnis, P., Lin, B., Yi, Y., Sun-Mack, S., Fan, T., and Ayers, J.:
567 Determination of ice water path in ice-over-water cloud systems using
568 combined MODIS and AMSR-E measurements, *Geophys. Res. Lett.*, 33,
569 L21801, doi:10.1029/2006GL027038, 2006.

570 Huang, J., Yu, H., Guan, X., Wang, G., and Guo, R.: Accelerated dryland expansion
571 under climate change, *Nature Climate Change*, 6, 166–171,
572 doi:10.1038/nclimate2837, 2016.

573 Jia, B., Xie, Z., Dai, A., Shi, C., and Chen F.: Evaluation of satellite and reanalysis
574 products of downward surface solar radiation over East Asia: Spatial and
575 seasonal variations, *J. Geophys. Res.-Atmos.*, 118, 3431–3446,
576 doi:10.1002/jgrd.50353, 2013.

577 Kawai, Y., and Kawamura H.: Validation and improvement of satellite derived surface
578 solar radiation over the northwestern Pacific Ocean, *J. Oceanogr.*, 61, 79–89,
579 doi:10.1007/s10872-005-0021-7, 2005.

580 Kim, D., and Ramanathan, V.: Solar radiation budget and radiative forcing due to
581 aerosols and clouds, *J. Geophys. Res.*, 113, D02203,
582 doi:10.1029/2007JD008434, 2008.

583 King, M. D., Tsay, S. C., Platnick, S. E., Wang, M. H., Liou, K. N.: Cloud retrieval
584 algorithms for MODIS: optical thickness, effective particle radius, and
585 thermodynamic phase, MODIS Algorithm Theoretical Basis Document No.
586 ATBD-MOD-05, 1997.

587 King, M., Menzel, W. P., Kaufman, Y. J., Tanre, D., Gao, B., Platnick, S.,

588 Ackerman , S. A., Remer, L. A., Pincus, R., Hubanks, P. K.: Cloud and aerosol
589 properties, precipitable water, and profiles of temperature and water vapor from
590 MODIS, IEEE T. Geosci. Remote, 41(2), 442–458,
591 doi:10.1109/TGRS.2002.808226, 2003.

592 Koepke, P., Hess, M., Schult, I., and Shettle, E. P.: Global Aerosol Data Set, Report
593 No. 243, Max-Planck Institut für Meteorologie, Hamburg, Germany, 1997.

594 Li, Y. Y., Yu, R. C., Xu, Y. P., Zhang, X. H.: Spatial distribution and seasonal
595 variation of cloud over China based on ISCCP data and surface observations, J.
596 Meteorol. Soc. Jpn., 82 (2), 761–773, 2004.

597 Li, Z., Cribb, M., Chang, F. L., Trishchenko, A., and Luo, Y.: Natural variability and
598 sampling errors in solar radiation measurements for model validation over the
599 atmospheric radiation measurement Southern Great Plains region, J. Geophys.
600 Res., 110, D15S19, doi:10.1029/2004JD005028, 2005.

601 Liang, S., Zheng, T., Liu, R. G., Fang, H. L., Tsay, S. C., and Running S.: Estimation
602 of incident photosynthetically active radiation from Moderate Resolution
603 Imaging Spectrometer data, J. Geophys. Res., 111, D15208,
604 doi:10.1029/2005JD006730, 2006.

605 Liu, S. M., Xu, Z., Zhu, Z., Jia, Z., Zhu, M.: Measurements of evapotranspiration
606 from eddy-covariance systems and large aperture scintillometers in the Hai
607 River Basin, China, J. Hydrol., 487, 24–38 doi:10.1016/j.jhydrol.2013.02.025,
608 2013.

609 Liu Y., Xia J., Shi C.-X., Hong Y.: An Improved Cloud Classification Algorithm for

610 China's FY-2C Multi-Channel Images Using Artificial Neural Network.
611 Sensors, 9, 5558-5579, 2009.

612 Lu, N., Liu, R., Liu, J., and Liang, S.: An algorithm for estimating downward
613 shortwave radiation from GMS 5 visible imagery and its evaluation over China, J.
614 Geophys. Res., 115, D18102, doi:10.1029/2009JD013457, 2010.

615 Lu, N., Qin, J., Yang, K., and Sun, J.: A simple and efficient algorithm to estimate daily
616 global solar radiation from geostationary satellite data, Energy, 36, 3179–3188,
617 doi:10.1016/j.energy.2011.03.007, 2011.

618 Ma, Y. and Pinker, R. T.: Modeling shortwave radiative fluxes from satellites, J.
619 Geophys. Res., 117, D23202, doi:10.1029/2012JD18332,1–19, 2012.

620 Minnis, P., Huang, J., Lin, B., Yi, Y., Arduini, R., Fan, T., Ayers, J., and Mace, G.:
621 Ice cloud properties in ice-over-water cloud systems using Tropical Rainfall
622 Measuring Mission (TRMM) visible and infrared scanner and TRMM
623 Microwave Imager data, J. Geophys. Res., 112 (D6), D06206,
624 doi:10.1029/2006JD007626, 2007.

625 Mondol, J. D., Yohanis, Y. G., Norton, B.: Solar radiation modelling for the
626 simulation of photovoltaic systems, Renew. Energ., 33(5), 1109–1120, 2008.

627 Mueller, R., Matsoukas, C., Gratzki, A., Behr, H., and Hollmann, R.: The CM-SAF
628 operational scheme for the satellite based retrieval of solar surface irradiance—A
629 LUT based eigenvector hybrid approach, Remote Sens. Environ., 113(5), 1012 –
630 1024, doi:10.1016/j.rse.2009.01.012, 2009.

631 Oliver M, Jackson T.: Energy and economic evaluation of building-integrated

632 photovoltaics. *Energy*, 26(4), 431–439, 2001.

633 Pinker, R. T., Tarpley, J. D., Laszlo, I., Mitchell, K. E., Houser, P. R., Wood, E. F.,
634 Schaake, J. C., Robock, A., Lohmann, D., Cosgrove, B. A., She_eld, J., Duan,
635 Q., Luo, L., and Higgins, R. W.: Surface radiation budgets in support of the
636 GEWEX Continental-Scale International Project (GCIP) and the GEWEX
637 Americas Prediction Project (GAPP), including the North American Land Data
638 Assimilation System (NLDAS) project, *J. Geophys. Res.*, 108, 8844,
639 doi:10.1029/2002JD003301, 2003.

640 Posselt, R., Mueller, R., Stöckli, R., & Trentmann, J.: Remote sensing of solar
641 surface radiation for climate monitoring–The CM-SAF retrieval in international
642 comparison, *Remote Sens. Environ.*, 118, 186–198, 2012.

643 Räisänen, P.: Two-stream approximations revisited: A new improvement and tests
644 with GCM data, *Q. J. Roy. Meteor. Soc.*, 128, 2397–2416, doi:
645 10.1256/qj.01.161, 2002.

646 Qin, J., Tang W. J., Yang, K., Lu N., Niu X. L., Liang, S. L.: An efficient
647 physically-based parameterization to derive surface solar irradiance based on
648 satellite atmospheric products, *J. Geophys. Res.-Atmos.*, 120, 4975–4988,
649 doi:10.1002/2015JD023097, 2015.

650 Rigollier, C., Lefèvre, M., and Wald, L.: The method Heliosat-2 for deriving
651 shortwave solar radiation from satellite images, *Sol. Energy*, 77(2), 159–169,
652 doi:10.1016/j.solener.2004.04.017, 2004.

653 Roebeling, R., van Putten, E., Genovese, G., Rosema, A.: Application of meteosat

654 derived meteorological information for crop yield predictions in Europe, *Int. J.*
655 *Remote Sens.*, 25(23), 5389–5401, 2004.

656 Schaaf, C.B., Gao, F., Strahler, A.H., Lucht, W., Li, X., Tsang, T., ... Roy, D.: First
657 operational BRDF, albedo nadir reflectance products from MODIS, *Remote*
658 *Sens. Environ.*, 83, 135–148, doi:10.1016/S0034-4257(02)00091-3, 2002.

659 Stackhouse, P. W., Gupta, S. K., Cox, S. J., Mikovitz, J. C., Zhang, T., and Chiacchio,
660 M.: 12-year surface radiation budget data set, *GEWEX News*, 14, 10–12, 2004.

661 Sun, Z., Liu, J., Zeng, X., and Liang H.: Parameterization of instantaneous global
662 horizontal irradiance: Cloudy-sky component, *J. Geophys. Res.*, 117, D14202,
663 doi:10.1029/2012JD017557, 2012.

664 Tanahashi, S., Kawamura, H., Matsuura, T., Takahashi, T., and Yusa H.: A system to
665 distribute satellite incident solar radiation in real-time, *Remote Sens. Environ.*,
666 75, 412–422, doi:10.1016/S0034-4257(00)00183-8, 2001.

667 Tang, W. J., Yang, K., He, J., and Qin, J.: Quality control and estimation of global
668 solar radiation in China, *Sol. Energy*, 84, 466–475, 2010.

669 Tang W. J., Yang K., Qin J., Min M.: Development of a 50-year daily surface solar
670 radiation dataset over China. *Sci. China Ser. D*, 56 (9), 1555–1565, doi:
671 10.1007/s11430-012-4542-9, 2013.

672 Wang H. M. and Pinker R.T.: Shortwave radiative fluxes from MODIS: Model
673 development and implementation, *J. Geophys. Res.*, 114, D20201,
674 doi:10.1029/2008JD010442, 2009.

675 Wang, P., Stammes, P., & Mueller, R.: Surface solar irradiance from SCIAMACHY

676 measurements: Algorithm and validation, *Atmos. Meas. Tech.*, 4, 875 – 891,
677 doi:10.5194/amt-4-875-2011, 2011.

678 Wang, P., Sneep, M., Veefkind, J.P., Stammes, P., & Levelt, P.F.: Evaluation of
679 broadband Surface solar irradiance from the Ozone Monitoring Instrument,
680 *Remote Sens. Environ.*, 149, 88 – 99, doi:10.1016/j.rse.2014.03.036, 2014.

681 Wu F. T., Fu C. B.: Assessment of GEWEX/SRB version 3.0 monthly global
682 radiation dataset over China, *Meteorol. Atmos. Phys.*, 112, 155-166, 2011.

683 Xue, B. L., Wang, L., Li, X., Yang, K., Chen, D. Sun, L.: Evaluation of
684 evapotranspiration estimates for two river basins on the Tibetan Plateau by a
685 water balance method, *J. Hydrol.*, doi: 10.1016/j.jhydrol.2013.04.005, 2013.

686 Yang, K., Koike, T., and Ye, B.: Improving estimation of hourly, daily, and monthly
687 solar radiation by importing global data sets, *Agr. Forest Meteorol.*, 137, 43–55,
688 2006.

689 Yang, K., Pinker, R. T., Ma, Y., Koike, T., Wonsick, M. M., Cox, S. J., Zhang, Y., and
690 Stackhouse P.: Evaluation of satellite estimates of downward shortwave
691 radiation over the Tibetan Plateau, *J. Geophys. Res.*, 113, D17204,
692 doi:10.1029/2007JD009736, 2008.

693 Yeom, J.M., Han, K.S.: Improved estimation of surface solar insolation using a
694 neural network and MTSAT-1R data, *Comput. Geosci.*, 36, 590–597, 2010.

695 Yeom, J.M., Han, K.S., Kim, Y.S., and Jang, J.D.: Neural network determination of
696 cloud attenuation to estimate insolation using MTSAT-1R data, *Int. J. Remote*
697 *Sens.*, 29 (21), 6193–6208, 2008.

698 Yu, R. C., Yu, Y. Q. and Zhang M. H.: Comparing cloud radiative properties between
699 the eastern China and the Indian monsoon region, *Adv. Atmos. Sci.*, 18 (6),
700 1090–1102, 2001.

701 Zhang, X. T., Liang, S. L., Zhou, G. Q., Wu, H. R., and Zhao, X.: Generating Global
702 LAnd Surface Satellite incident shortwave radiation and photosynthetically
703 active radiation products from multiple satellite data, *Remote Sens. Environ.*,
704 152, 318-332, 2014.

705 Zhang, Y., Rossow, W. B., Lacis, A. A., Oinas, V., and Mishchenko, M. I.:
706 Calculation of radiative fluxes from the surface to top of atmosphere based on
707 ISCCP and other global data sets-refinements of the radiative transfer model
708 and the input data, *J. Geophys. Res.*, 109, D19105, doi:10.1029/2003JD004457,
709 2004.

710 **Figure captions**

711 **Figure 1** Spatial distribution of ground stations used for SSR retrieval validation.

712 The Red Cross marks illustrate the 44 BSRN stations, the Blue Cross
713 marks denote three experimental stations over Haihe River Basin in China,
714 and the Circle marks represent the 90 CMA radiation stations.

715 **Figure 2** Flowchart of the SSR retrieval algorithm.

716 **Figure 3** Comparisons of water Cloud parameters between the MODIS “true values”
717 and the estimated ones by ANN for (a) effective particle radius and (b)
718 liquid water path.

719 **Figure 4** Same as Figure 3, but for ice cloud.

720 **Figure 5** (a) Sensitivity of SSR to cloud liquid/ice water path, given the effective
721 particle radius for water cloud and ice cloud to be 12 μm and 30 μm ,
722 respectively; (b) Sensitivity of SSR to cloud effective particle radius for
723 water cloud and ice cloud, given liquid/ice water path to be 80 g m^{-2} .

724 **Figure 6** Validation of instantaneous SSR estimated with the MODIS atmospheric
725 and land products against the observed ones at 44 BSRN stations in 2009
726 for (a) Terra and (b) Aqua platforms. Unit of MBE and RMSE is W m^{-2} .

727 **Figure 7** Comparison between the observed and the estimated hourly SSR at three
728 experimental stations over Haihe River Basin in 2009. Unit of MBE and
729 RMSE is W m^{-2} .

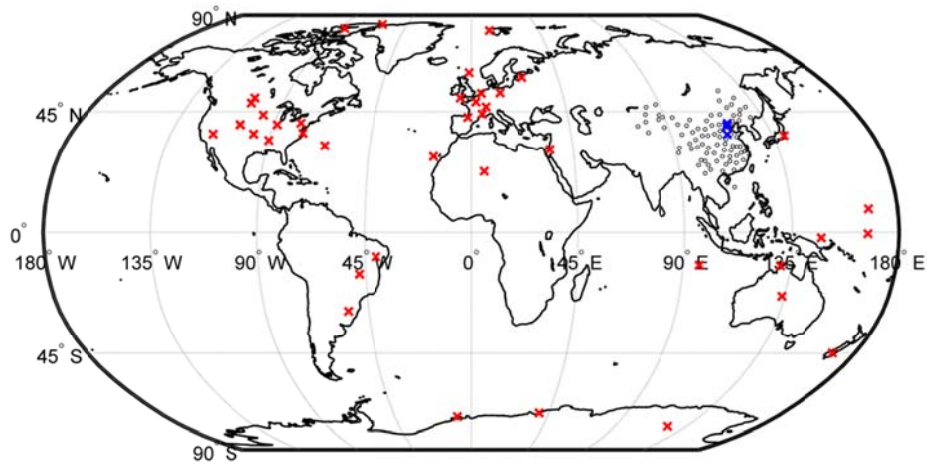
730 **Figure 8** (a) Comparison between the observed and the estimated daily SSR at all
731 CMA radiation stations in 2009. (b) Similar to panel (a), but for monthly

732 SSR. Unit of MBE and RMSE is $W m^{-2}$.

733 **Figure 9** Spatial distributions of MBE and RMSE for daily and monthly SSR
734 estimates at all CMA radiation stations in 2009, respectively. The size of
735 the circles is corresponding to the MBE and RMSE values. The solid circle
736 means that the MBE is greater than zero, and the open circle means that
737 the MBE is less than zero. The units of RMSE and MBE described on the
738 legend are in $W m^{-2}$.

739 **Figure 10** Comparison between the observed and the estimated daily SSR at all
740 CMA radiation stations in 2009 for (a) This study, (b) The GLASS and (c)
741 ISCCP-FD. Unit of MBE and RMSE is $W m^{-2}$.

742 **Figure 11** SSR estimates for 12 months in 2009 over the mainland China. The unit
743 of the SSR is $W m^{-2}$, and the pixel size is about 5 km.



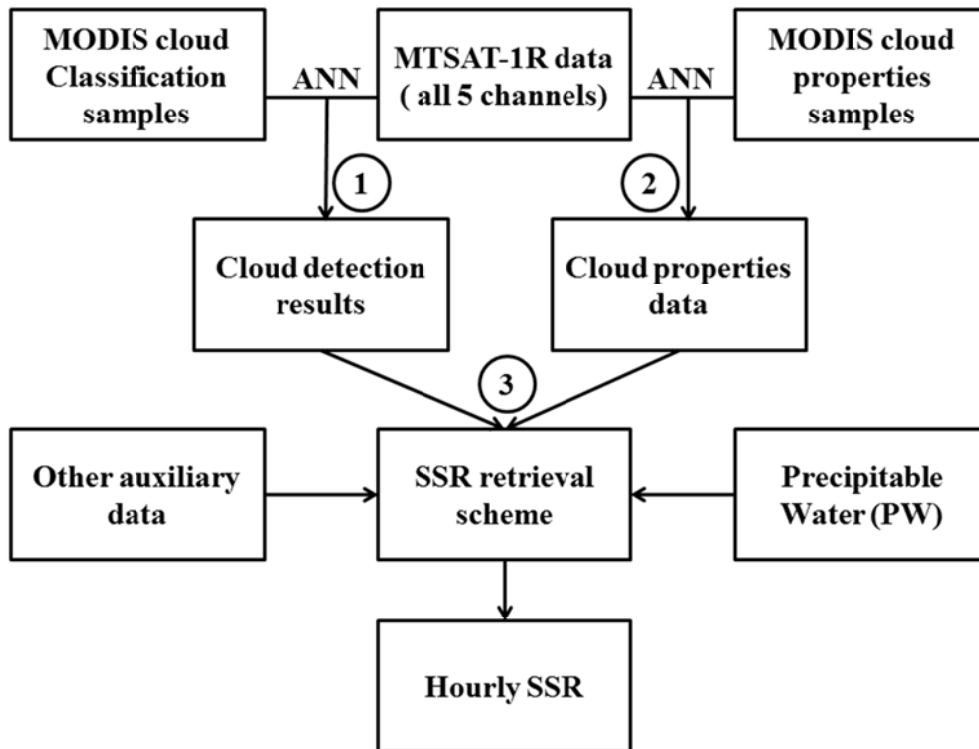
745

749 **Figure 1** Spatial distribution of ground stations used for SSR retrieval validation. The

750 Red Cross marks illustrate the 44 BSRN stations, the Blue Cross marks

751 denote three experimental stations over Haihe River Basin in China, and the

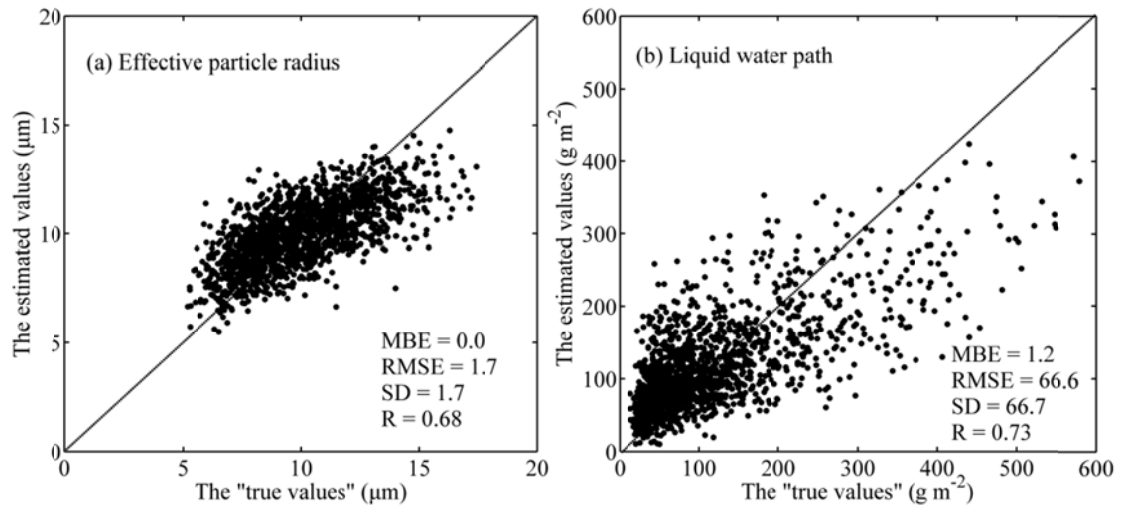
752 Circle marks represent the 90 CMA radiation stations.



750

751

Figure 2 Flowchart of the SSR retrieval algorithm.

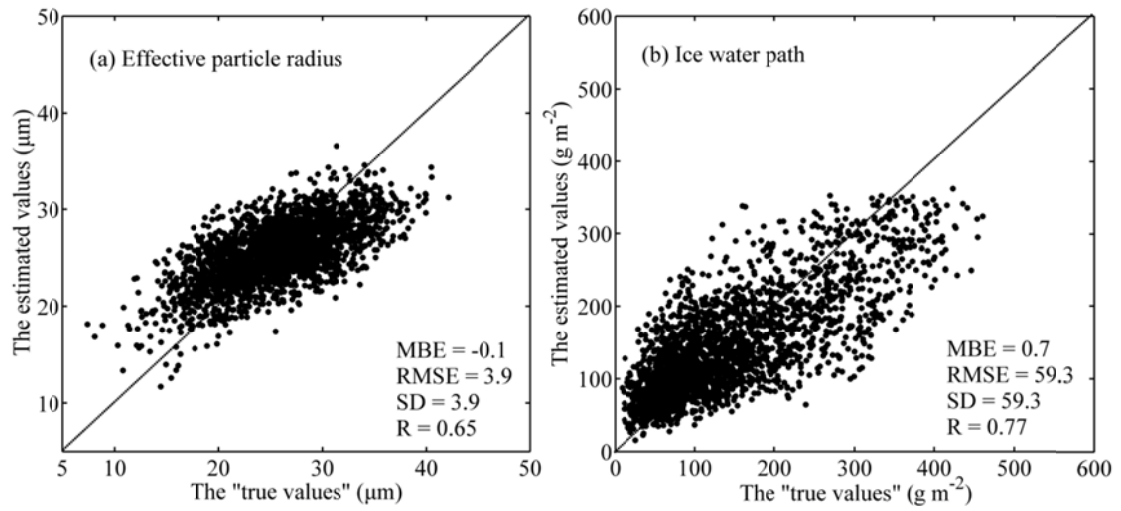


752

755 **Figure 3** Comparisons of water cloud parameters between the MODIS “true values”

756 and the estimated ones by ANN for (a) effective particle radius and (b)

757 liquid water path.

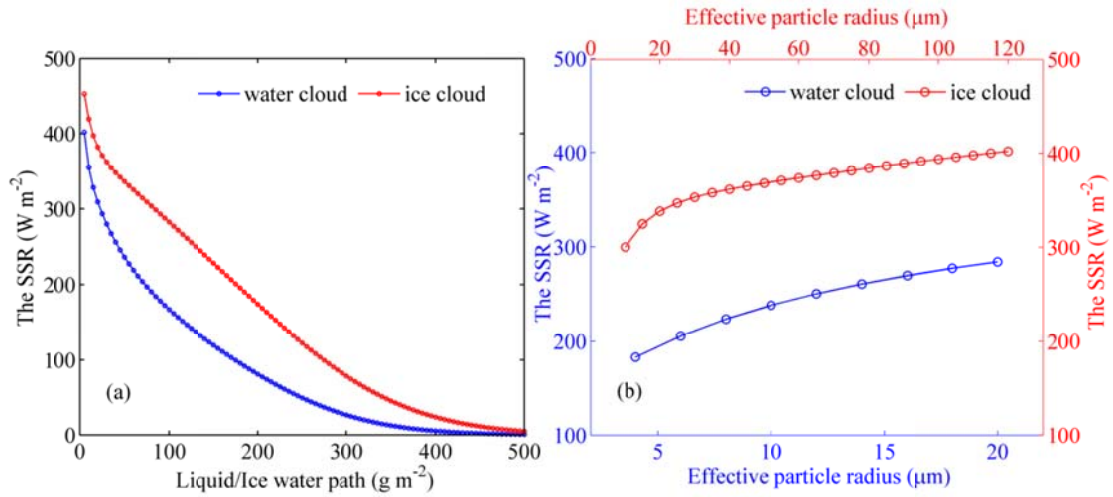


756

757

Figure 4 Same as Figure 3, but for ice cloud.

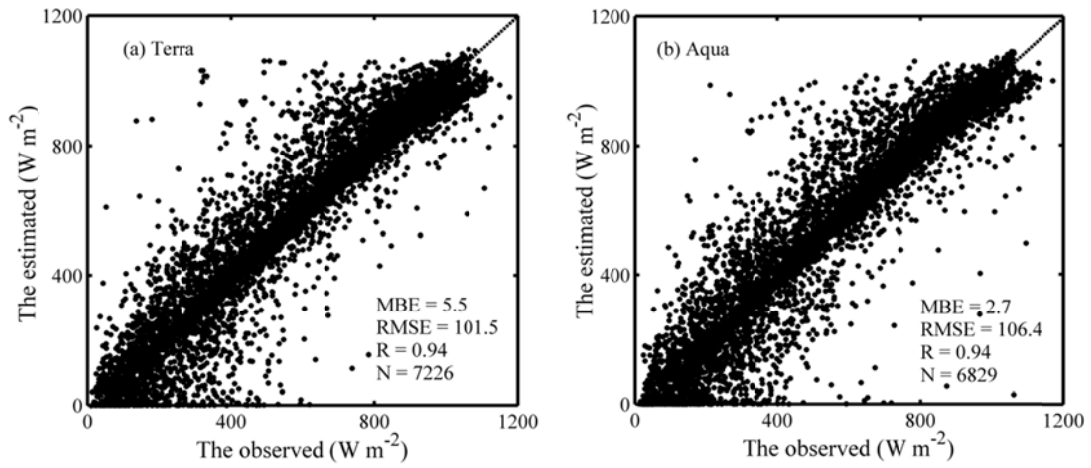
758



759

763 **Figure 5** (a) Sensitivity of SSR to cloud liquid/ice water path, given the effective
 764 particle radius for water cloud and ice cloud to be 12 μm and 30 μm ,
 765 respectively; (b) Sensitivity of SSR to cloud effective particle radius for
 766 water cloud and ice cloud, given liquid/ice water path to be 80 $g m^{-2}$.

764

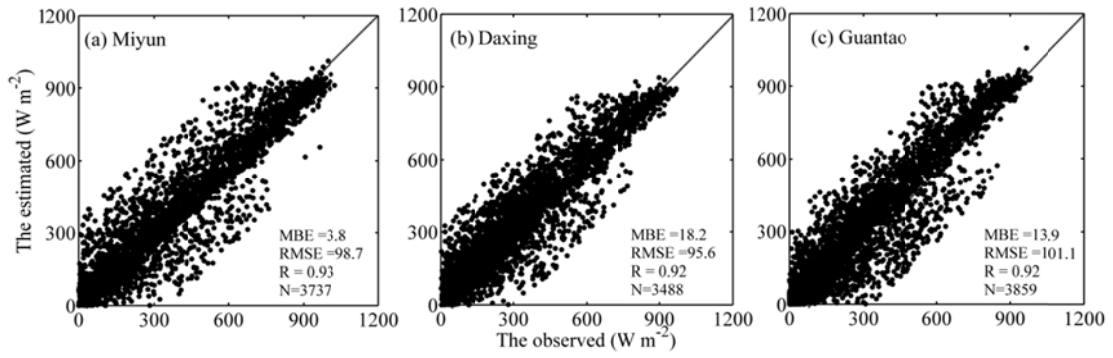


765

768 **Figure 6** Validation of instantaneous SSR estimated with the MODIS atmospheric

769 and land products against the observed ones at 44 BSRN stations in 2009

770 for (a) Terra and (b) Aqua platforms. Unit of MBE and RMSE is $W m^{-2}$.

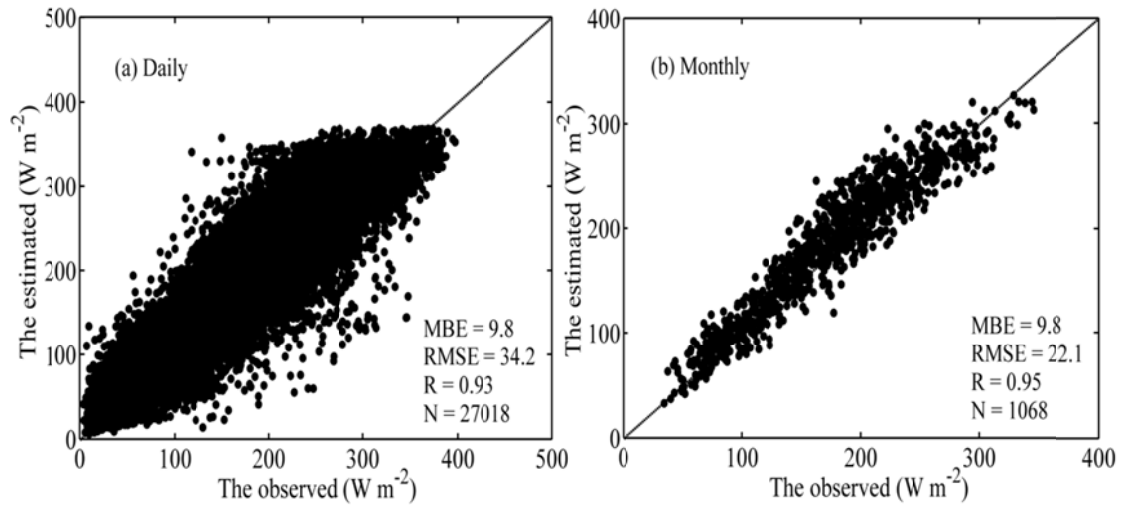


769

772 **Figure 7** Comparison between the observed and the estimated hourly SSR at three

773 experimental stations over Haihe River Basin in 2009. Unit of MBE and

774 RMSE is $W m^{-2}$. Points outside 3-std were removed (about 1.88%).

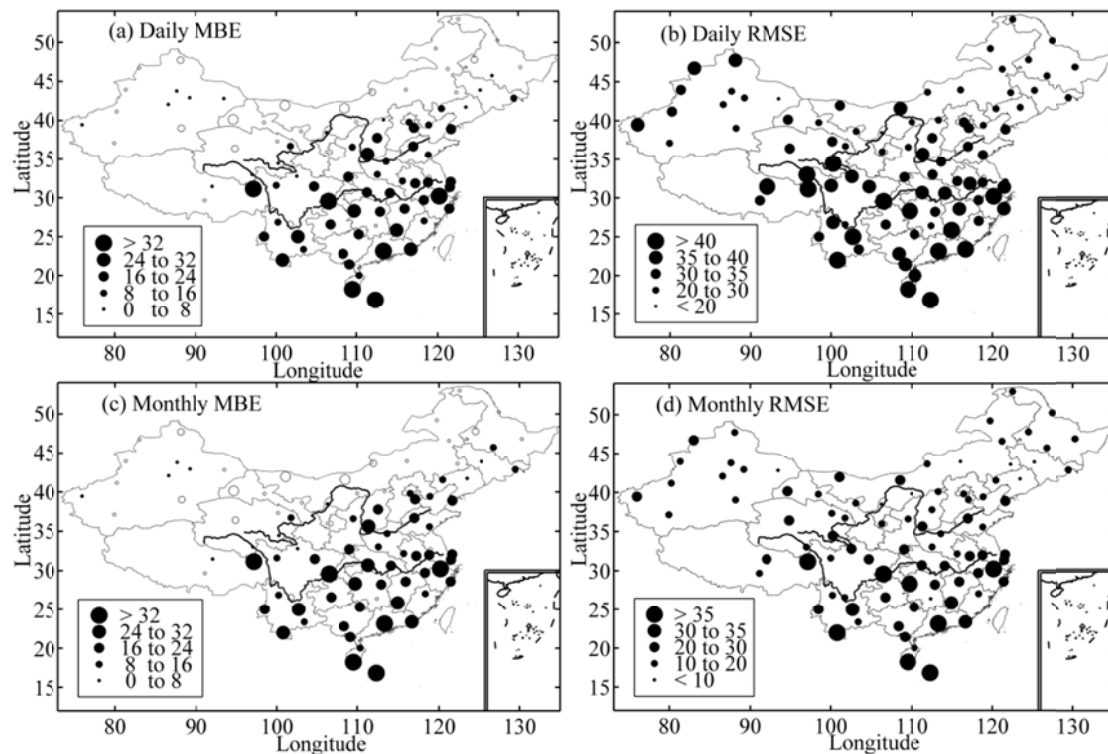


773

776 **Figure 8 (a)** Comparison between the observed and the estimated daily SSR at all

777 CMA radiation stations in 2009; **(b)** Similar to panel (a), but for monthly

778 SSR. Unit of MBE and RMSE is $W m^{-2}$.



777

783 **Figure 9** Spatial distributions of MBE and RMSE for daily and monthly SSR

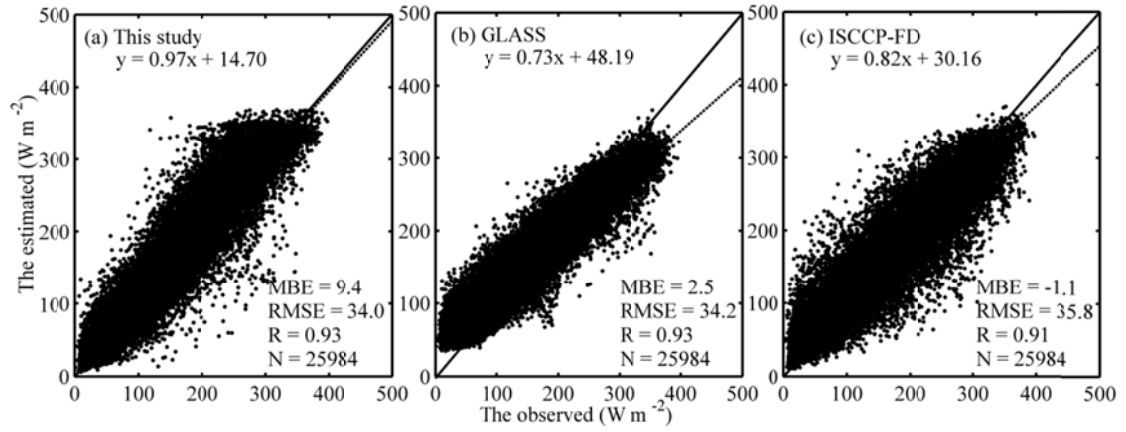
784 estimates at all CMA radiation stations in 2009, respectively. The size of

785 the circles is corresponding to the MBE and RMSE values. The solid circle

786 means that the MBE is greater than zero, and the open circle means that

787 the MBE is less than zero. The units of RMSE and MBE described on the

788 legend are in $W m^{-2}$.



784

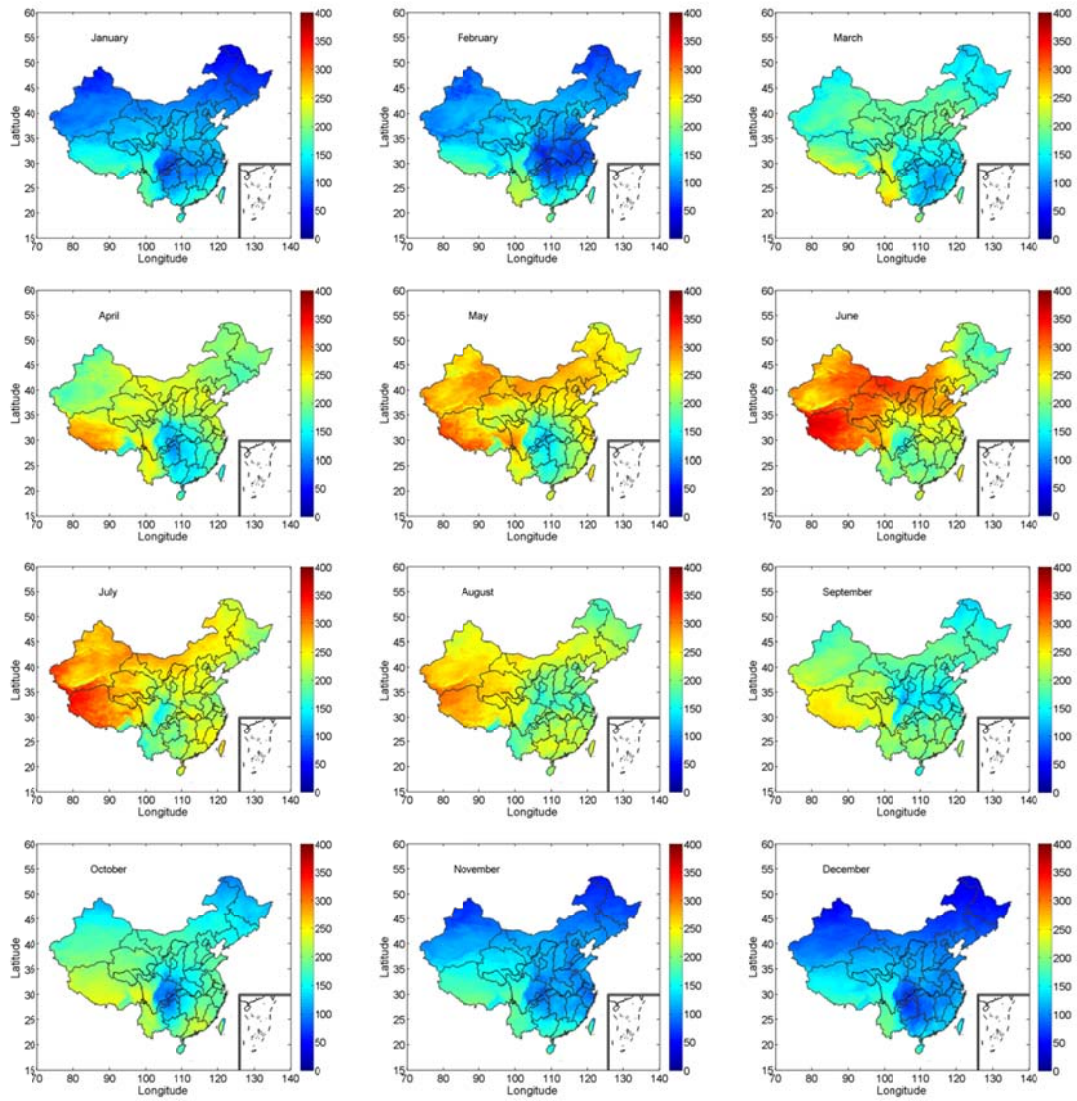
787 **Figure 10** Comparison between the observed and the estimated daily SSR at all

788

CMA radiation stations in 2009 for (a) This study, (b) The GLASS and (c)

789

ISCCP-FD. Unit of MBE and RMSE is $W m^{-2}$.



788

790 **Figure 11** SSR estimates for 12 months in 2009 over the mainland China. The unit

791

of the SSR is W m^{-2} , and the pixel size is about 5 km.

Table 1 Characteristics of MTSAT bands used in this study.

Channel	Band Wavelength (μm)	Resolution at nadir (km)
VIS	0.55-0.90	1.0×1.0
IR-1	10.3-11.3	4.0×4.0
IR-2	11.5-12.5	4.0×4.0
IR-3	6.5-7.0	4.0×4.0
IR-4	3.5-4.0	4.0×4.0

791 **Table 2** The basic information of three experimental stations over Haihe River Basin.

Station Name	Latitude (°N)	Longitude (°E)	Altitude (m)	Instrument height (m)
Miyun	40.6	117.3	350	30.8
Daxing	39.6	116.4	20	28.0
Guantao	36.5	115.1	30	15.7

792